Accurate ab initio potential energy surface, thermochemistry, and dynamics of the Cl(2P, 2P3/2) + CH4 → HCl + CH3 and H + CH3Cl reactions

Gábor Czakó and Joel M. Bowman

Citation: J. Chem. Phys. **136**, 044307 (2012); doi: 10.1063/1.3679014
View online: http://dx.doi.org/10.1063/1.3679014
View Table of Contents: http://jcp.aip.org/resource/1/JCPSA6/v136/i4
Published by the American Institute of Physics.

Accurate *ab initio* potential energy surface, thermochemistry, and dynamics of the $Cl(^2P, ^2P_{3/2}) + CH_4 \rightarrow HCl + CH_3$ and $H + CH_3Cl$ reactions

Gábor Czakó[a] and Joel M. Bowman
Cherry L. Emerson Center for Scientific Computation and Department of Chemistry, Emory University, Atlanta, Georgia 30322, USA

(Received 26 October 2011; accepted 3 January 2012; published online 25 January 2012)

We report a high-quality, *ab initio*, full-dimensional global potential energy surface (PES) for the $Cl(^2P, ^2P_{3/2}) + CH_4$ reaction, which describes both the abstraction ($HCl + CH_3$) and substitution ($H + CH_3Cl$) channels. The analytical PES is a least-squares fit, using a basis of permutationally invariant polynomials, to roughly 16 000 *ab initio* energy points, obtained by an efficient composite method, including counterpoise and spin-orbit corrections for the entrance channel. This composite method is shown to provide accuracy almost equal to all-electron CCSD(T)/aug-cc-pCVQZ results, but at much lower computational cost. Details of the PES, as well as additional high-level benchmark characterization of structures and energetics are reported. The PES has classical barrier heights of 2650 and 15 060 cm^{-1} (relative to $Cl(^2P_{3/2}) + CH_4(eq)$), respectively, for the abstraction and substitution reactions, in good agreement with the corresponding new computed benchmark values, 2670 and 14 720 cm^{-1}. The PES also accurately describes the potential wells in the entrance and exit channels for the abstraction reaction. Quasiclassical trajectory calculations using the PES show that (a) the inclusion of the spin-orbit corrections in the PES decreases the cross sections by a factor of 1.5–2.5 at low collision energies (E_{coll}); (b) at $E_{coll} \approx 13\,000$ cm^{-1} the substitution channel opens and the H/HCl ratio increases rapidly with E_{coll}; (c) the maximum impact parameter (b_{max}) for the abstraction reaction is ~6 bohr; whereas b_{max} is only ~2 bohr for the substitution; (d) the HCl and CH_3 products are mainly in the vibrational ground state even at very high E_{coll}; and (e) the HCl rotational distributions are cold, in excellent agreement with experiment at $E_{coll} = 1280$ cm^{-1}.
 [doi:10.1063/1.3679014]

I. INTRODUCTION

In order to gain understanding of the dynamics of polyatomic bimolecular reactions in the gas phase, the reactions of methane with F and Cl atoms have been extensively studied both experimentally and theoretically.[1–12] Following the early work on mode-specific dynamics of Cl + methane, performed in the groups of Crim,[2,3] Zare,[13] and Orr-Ewing,[14] Liu and coworkers[1,7] carried out crossed molecular beam experiments for both reactions, where they have been able to measure the correlated distributions of the product vibrational states. These experiments uncovered surprising results, namely, that (a) CH-stretching excitation enhances the DF + CHD_2 products in the F + CHD_3 reaction[1] and (b) the CH-stretching excitation energy is no more effective to activate the late-barrier Cl + CHD_3 reaction than the translational energy,[7] contradicting the Polanyi rules.[15]

The first-principles computations of the above-mentioned correlated distributions, as well as the simulations of the experimental results, are challenging, but there has been progress toward accurate dynamical calculations for the F and Cl + methane reactions. In 2009 we developed a full-dimensional, *ab initio* potential energy surface (PES) for the F + CH_4 reaction,[8] which was recently improved by developing an *ab initio* spin-orbit (SO) correction surface to the PES.[16] Quasiclassical trajectory (QCT) calculations[8] on this PES provided HF(v,J) ro-vibrational distributions in excellent agreement with experiments of Nesbitt and co-workers.[17] These results demonstrated the utility of QCT and the importance of an accurate PES. Furthermore, we found that the CH-stretching excitation steers the slow F atom to the CD bond in the F + CHD_3 reaction supporting the above-mentioned surprising experimental finding.[1,9] Very recently, we reported a high-quality, full-dimensional, SO-corrected, *ab initio* PES for the Cl + CH_4 reaction.[18] Both the F and Cl + CH_4 PESs are permutationally invariant fits to high-level *ab initio* electronic energies obtained by efficient composite methods as discussed in detail in Sec. III.

Since the first *ab initio* study[19] of the Cl + CH_4 reaction published in 1989, several PESs have been reported for this reaction describing the abstraction channel. In 1996 Espinosa-García and Corchado[20] developed a semi-empirical PES by adjusting the parameters of an earlier H + CH_4 surface.[21] This PES was further improved in 2000 (Ref. 22) based on thermal rate constants and in 2006 (Ref. 23) using *ab initio* stationary point properties in addition to the measured thermal data. In 1999 Yu and Nyman[24] reported the first *ab initio* PES using a three-degree-of-freedom model. In 2007 Banks and Clary[25] developed a two-dimensional (2D) *ab initio* non-SO PES and very recently in 2011 they reported PESs for all the SO states, again in a 2D model.[26] The first full-dimensional *ab initio* PES was developed in

[a]Author to whom correspondence should be addressed. Electronic mail: czako@chem.elte.hu.

2006 by Castillo *et al.*[27] using Shepard interpolation and the QCISD/aug-cc-pVDZ + scaling-all-correlation level of theory. Also in that year, Troya and Weiss[12] reported a specific reaction parameter (SRP) semi-empirical Hamiltonian (SRP-MSINDO) for the Cl + CH_4 reaction allowing efficient on-the-fly computation of the PES. In 2011 Greaves *et al.*[28] showed that another semi-empirical Hamiltonian (SRP-AM1), which was previously optimized for the Cl + ethane reaction, can be used for the title reaction.

Following our earlier work on F + CH_4,[8] the present Cl + CH_4 PES development uses an efficient composite electronic structure method. Composite *ab initio* methods have been widely and successfully used for thermochemical[29–32] and spectroscopic[33] applications; in this paper we demonstrate their utility for polyatomic reaction dynamics studies. As a result, this Cl + CH_4 PES incorporates (a) basis set effects up to aug-cc-pCVTZ (correlation-consistent polarized core-valence triple-zeta basis augmented with diffuse functions);[34] (b) electron correlation up to the "gold standard" CCSD(T) method;[35] (c) the core-core and core-valence correlation effects; and (d) SO and counterpoise corrections for the entrance channel. Furthermore, the present PES describes both the major abstraction (HCl + CH_3) channel as well as the high-energy substitution (H + CH_3Cl) channel.

Here, we report a detailed description of this PES and its *ab initio* characterization. The present study also provides new *ab initio* benchmark values for the energetics of the title reactions. We focus especially on the wells in the entrance and exit channels and resolve the conflicting conclusions in the literature regarding the well depth and its dependence on the orientation of the reactants for the former well. The benchmark barrier heights and reaction energies are obtained by the composite focal point analysis (FPA) approach,[29,30] which considers a number of effects, such as (a) extrapolations to the complete basis set (CBS) limit using aug-cc-pV*X*Z [*X* = 5, 6] bases, (b) electron correlation beyond CCSD(T), (c) core electron correlation effects, (d) scalar relativistic effects, and (e) SO corrections, which were routinely neglected in previous studies.

After presenting the benchmark structures and energetics in Sec. II, we describe the computational details of the PES development in Sec. III. We show the accuracy of the composite method applied for the computation of roughly 16 000 electronic energies. Then we give the details of the global fit, which provides an analytical representation of the PES based on polynomials that are invariant under permutations of like atoms.[36,37] In Sec. III we demonstrate the accuracy of the PES by comparing the structures, energetics, and frequencies to the new benchmark values. In Sec. IV QCT calculations are reported for the Cl + CH_4 reaction, using the non-SO and SO-corrected PESs. We focus on two main aspects of the dynamics, which, to the best of our knowledge, have not been studied before. First, we investigate both the HCl + CH_3 abstraction channel and the high-energy H + CH_3Cl substitution channel. The latter has high barrier (14 720 cm^{-1}); thus, it is closed at low collision energies. We consider collision energies up to 20 000 cm^{-1}; thus, we can calculate the branching ratios of the H/HCl products. Second, we show the effect of the inclusion of the SO correction in the PES by comparing reaction cross sections obtained on the non-SO and SO PESs. We also show a comparison between the computed and measured HCl rotational distributions and also give the mode-specific vibrational energy distribution of the CH_3 product. Finally, a summary and conclusions are presented in Sec. V.

II. *AB INITIO* CHARACTERIZATION

A. Computational details

The benchmark electronic structure computations employed the augmented correlation-consistent polarized (Core-)Valence *X* Zeta basis sets, specifically the aug-cc-pV*X*Z [*X* = 2(D), 3(T), 4(Q), 5, 6] and aug-cc-pCV*X*Z [*X* = 2(D), 3(T), 4(Q)] bases.[38–40] For the single-reference correlation methods the reference electronic wave functions were determined by the single-configuration restricted, as well as unrestricted, open-shell Hartree–Fock (ROHF and UHF) methods.[41] For treating electron correlation we used the restricted and unrestricted open-shell second-order Møller–Plesset perturbation theory (RMP2 and UMP2) (Ref. 42) and the coupled-cluster (CC) (Ref. 43) methods including all single and double (CCSD) and triple (CCSDT) excitations as well as the CCSD(T) (Refs. 35 and 44) and CCSDT(Q) (Ref. 45) methods including perturbative triple (T) and quadruple (Q) terms. For open-shell systems the CC computations employ the ROHF-UCCSD and ROHF-UCCSD(T) formalism, whereas the post-UCCSD(T) computations were performed based on UHF orbitals. The two different formalisms provide the same energies within 1–5 cm^{-1}; therefore, in the following text the UCCSD, UCCSD(T), etc. abbreviations will be used regardless of the reference orbitals, which are precisely defined above. Finally, we note that in this study FC denotes the use of the usual frozen-core approach for the electron correlation calculations, while AE means computations when all the electrons are correlated.

All the electronic structure computations up to UCCSD(T), including geometry optimizations, harmonic frequency calculations, and single-point energy computations, were performed using MOLPRO.[46] The MRCC program[47,48] (interfaced to CFOUR (Ref. 49)) was employed for UCCSDT and UCCSDT(Q). Some of the large UCCSDT computations were performed by CFOUR. The scalar relativistic effects were computed using Douglas–Kroll[50] relativistic one-electron integrals as implemented in MOLPRO. The multi-reference configuration interaction (MRCI + Q) computations using the Davidson correction to estimate the effect of the higher order excitations (+Q) as well as the spin-orbit calculations with the Breit–Pauli operator in the interacting states approach[51] were also performed by MOLPRO. These MRCI calculations utilized an active space of 5 electrons in the 3 spatial 3p-like orbitals corresponding to the Cl atom.

The benchmark relative energies were determined following the FPA approach.[29,30] The FPA employs the best reference structures, i.e., geometries obtained at AE-UCCSD(T) with aug-cc-pCVTZ, aug-cc-pCVQZ, and aug-cc-pCVQZ for the barrier height, dissociation energy, and reaction enthalpy calculations, respectively. Single-point electronic structure

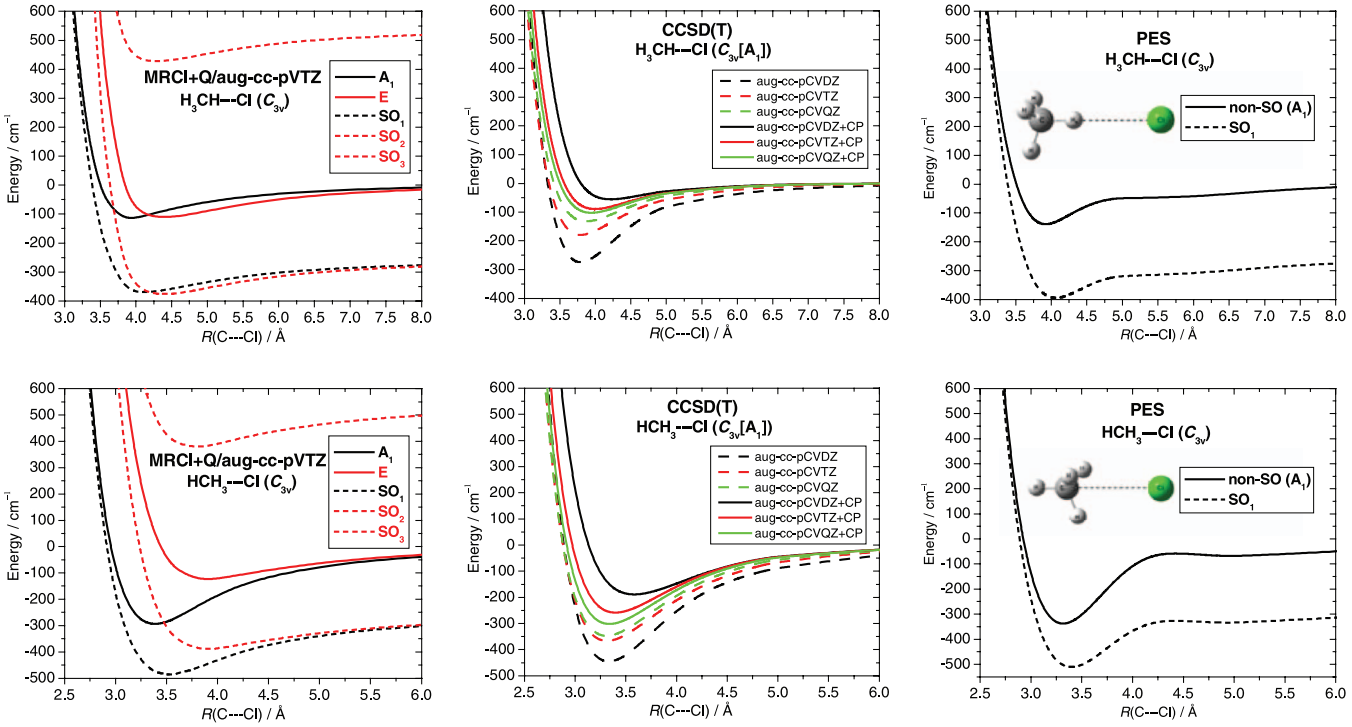

FIG. 1. Potential energy curves of CH_4–Cl as a function of the C–Cl distance along the C_{3v} axis with fixed CH_4(eq) geometry and CH–Cl (upper panels) and HC–Cl (lower panels) linear bond arrangements computed at the frozen-core MRCI + Q/aug-cc-pVTZ level (left panels) and all-electron CCSD(T)/aug-cc-pCVXZ (X = D, T, Q) level, where +CP indicates the use of the counterpoise correction (middle panels). The right panels show the potential curves obtained from the non-SO and SO-corrected ground state PESs. A_1 and E denote the ground and excited non-SO electronic states, respectively, and SO_1, SO_2, SO_3 are the three spin-orbit states. The middle panels show the A_1 state only at different levels of theory. The energies are relative to Cl(^{2}P) + CH_4(eq). The data shown in the left and right panels were also reported in Fig. 2 in Ref. 18.

computations were performed at the above-defined reference structures considering (a) extrapolations to the CBS limit using aug-cc-pVXZ [X = 5, 6] bases; (b) electron correlation beyond UCCSD(T) by performing UCCSDT/aug-cc-pVTZ and UCCSDT(Q)/aug-cc-pVDZ (in some cases UCCSDT(Q)/aug-cc-pVTZ) computations; (c) core electron correlation effects as difference between AE and FC UCCSD(T)/aug-cc-pCVQZ energies; (d) scalar relativistic effects at AE Douglas–Kroll UCCSD(T)/aug-cc-pCVQZ level; and (e) SO corrections obtained from the experimentally known SO splitting of the Cl atom.

The ROHF energies, E_X^{HF}, and the electron correlation energy increments, $E_X^{\mathrm{corr.}}$, obtained by the corresponding aug-cc-pVXZ basis set, have been extrapolated to determine the CBS limits, $E_{\mathrm{CBS}}^{\mathrm{HF}}$ and $E_{\mathrm{CBS}}^{\mathrm{corr.}}$, respectively, employing two-parameter formulas,[52,53]

$$E_X^{\mathrm{HF}} = E_{\mathrm{CBS}}^{\mathrm{HF}} + a(X+1)e^{-9\sqrt{X}} \quad (1)$$

and

$$E_X^{\mathrm{corr.}} = E_{\mathrm{CBS}}^{\mathrm{corr.}} + bX^{-3}. \quad (2)$$

In order to get the best estimates for the CBS limits using the above asymptotic formulas, the best two energies were used in the extrapolations, which means the X = 5 and 6 values up to UCCSD and X = 4 and 5 for some of the UCCSD(T) energy increments.

B. Entrance channel van der Waals region

Figure 1 presents the potential curves for the entrance channel showing the van der Waals (vdW) well with CH–Cl and HC–Cl C_{3v} bond arrangements. There are contradictions in the literature on the depth of this well. A study reported that the well at both configurations is about 100 cm^{-1} deep,[12] in disagreement with the present results. We found that a source of these contradictions is that two electronic states are close to each other at this region (see Fig. 1, left panels) and a single-reference *ab initio* method can fail to converge to the right state. The present MRCI + Q results show that the excited electronic state has minima along the C_{3v} axis with CH–Cl and HC–Cl bond arrangements with depths of about 100 cm^{-1} for both, whereas the electronic ground state gives well depths of 100 and 300 cm^{-1}, respectively. Furthermore, the SO correction decreases the depth of the latter by 100 cm^{-1}, but the HC–Cl vdW well still remains the deeper minimum. In order to benchmark the above energies we performed AE-CCSD(T)/aug-cc-pCVXZ [X = D, T, Q] computations for the electronic ground state potential with and without counterpoise corrections for the basis set superposition error (BSSE). As Fig. 1 (middle) shows the aug-cc-pCVDZ basis provides too deep vdW minima due to the large BSSE; however, the computed counterpoise correction overestimates the BSSE and gives too shallow vdW region. As the basis size is increased to TZ and QZ we see that the potentials with and without BSSE correction converge to each other as seen in Fig. 1 (middle panels). We found very good agreement

TABLE I. Structure (in Å and degrees) and classical barrier height (V_{SP}, cm^{-1}) for the abstraction saddle point $(CH_3–H_b–Cl)_{SP}$ at different levels of theory.

Methods[a]	r(CH)	r(CH_b)	r(H_bCl)	α(HCH_b)	V_{SP}
FC-UMP2/aug-cc-pVDZ	1.093	1.368	1.463	101.2	2754
FC-UMP2/aug-cc-pVTZ	1.081	1.352	1.457	101.6	2557
FC-UMP2/aug-cc-pVQZ	1.080	1.343	1.460	101.6	2370
AE-UMP2/aug-cc-pCVDZ	1.092	1.360	1.464	101.3	2529
AE-UMP2/aug-cc-pCVTZ	1.080	1.340	1.458	101.7	2357
AE-UMP2/aug-cc-pCVQZ	1.078	1.333	1.462	101.7	2236
FC-UCCSD(T)/aug-cc-pVDZ	1.097	1.419	1.451	100.7	2830
FC-UCCSD(T)/aug-cc-pVTZ	1.084	1.407	1.443	101.0	2711
AE-UCCSD(T)/aug-cc-pCVDZ	1.096	1.413	1.451	100.8	2649
AE-UCCSD(T)/aug-cc-pCVTZ	1.083	1.397	1.443	101.1	2577

[a]FC and AE denote frozen-core and all-electron computations, respectively.

between the benchmark AE-CCSD(T)/aug-cc-pCVQZ and the MRCI + Q/aug-cc-pVTZ ground state potentials, indicating that the presented MRCI + Q potential curves are reasonably accurate for all the non-relativistic and SO states.

C. The Cl + CH_4 → HCl + CH_3 reaction

The structures of the first-order saddle point $(CH_3–H_b–Cl)_{SP}$, complex in the product channel (CH_3–HCl), and the reactant and products computed at different levels of theory are given in Tables I and II. The benchmark FPA results for the classical barrier height, D_e of (CH_3–HCl), and reaction endoergicity are given in Tables III–V.

The abstraction reaction has a late barrier, i.e., product-like structure, as seen in Fig. 2. Indeed, the C–H_b distance (1.397 Å) is significantly stretched by 0.309 Å relative to the CH bond length in CH_4. The H_b–Cl distance is 1.443 Å at the saddle point, which is longer than the bond length of the HCl molecule by only 0.168 Å. The UMP2 method gives reasonable estimates for the saddle-point structure; it underestimates the C–H_b distance by about 0.05 Å and overestimates the H_b–Cl distance by about 0.01 Å relative to the UCCSD(T) results. The point-group symmetry of the saddle-point structure is C_{3v} regardless the level of theory. Note that for F + CH_4 the saddle point has C_{3v} symmetry at UMP2 level, whereas the more accurate UCCSD(T) method gives C_s saddle-point structure with α(C–H_b–F) ≈ 150°.[8] This bent saddle-point structure is unique for F + CH_4 among the halogen + CH_4 reactions, since our recent computations showed that the Br and I + CH_4 reactions have collinear C_{3v} saddle points,[54] similar to Cl + CH_4. Our best estimate for the classical barrier height is 2670 ± 40 cm^{-1}. (Note that the uncertainty is based on the results obtained at systematically increased levels of *ab initio* method and basis as shown in Table III.) Electron correlation plays an important role in the accurate determination of this key energy. The ROHF method overestimates the barrier by roughly 6600 cm^{-1}, UMP2 underestimates it by ∼400 cm^{-1}, and UCCSD overestimates it significantly by ∼900 cm^{-1}. One has to employ at least the UCCSD(T) method to achieve reasonable convergence; the post-UCCSD(T) correlation contribution is only about −40 cm^{-1} based on the UCCSDT and UCCSDT(Q) computations. There is also a significant basis set dependence on the barrier height. The aug-cc-pV*X*Z bases overestimate the barrier by 340, 270, and 70 cm^{-1} for X = D, T, and Q, respectively. The contributions of the core electron correlation

TABLE II. Equilibrium structures (in Å and degrees) of the reactant, products, and the exit-channel complex (CH_3–HCl) as well as relative energies at different levels of theory for the $Cl(^2P) + CH_4 \rightarrow HCl + CH_3$ reaction.

	Cl + CH_4	(CH_3–HCl) (C_{3v})					HCl + CH_3 (D_{3h})		
Methods[a]	r(CH)	r(CH)	r(CH_b)	r(H_bCl)	α(HCH_b)	D_e[b]	r(CH)	r(HCl)	ΔE_e[b]
FC-UMP2/aug-cc-pVDZ	1.098	1.089	2.247	1.297	93.0	946	1.088	1.288	2148
FC-UMP2/aug-cc-pVTZ	1.086	1.076	2.203	1.286	93.0	916	1.075	1.275	1831
FC-UMP2/aug-cc-pVQZ	1.085	1.075	2.206	1.285	92.8	881	1.073	1.273	1570
AE-UMP2/aug-cc-pCVDZ	1.097	1.088	2.239	1.296	93.0	1011	1.086	1.286	1989
AE-UMP2/aug-cc-pCVTZ	1.085	1.075	2.199	1.282	93.0	925	1.074	1.271	1549
AE-UMP2/aug-cc-pCVQZ	1.083	1.073	2.211	1.281	92.8	875	1.072	1.270	1347
FC-UCCSD(T)/aug-cc-pVDZ	1.103	1.094	2.282	1.300	92.9	917	1.093	1.292	2417
FC-UCCSD(T)/aug-cc-pVTZ	1.090	1.081	2.223	1.289	93.0	879	1.080	1.279	2247
FC-UCCSD(T)/aug-cc-pVQZ	1.088	1.079	2.236	1.288	92.6	839	1.078	1.278	1963
AE-UCCSD(T)/aug-cc-pCVDZ	1.101	1.093	2.269	1.299	92.9	978	1.092	1.290	2296
AE-UCCSD(T)/aug-cc-pCVTZ	1.088	1.079	2.230	1.285	92.8	884	1.078	1.275	2038
AE-UCCSD(T)/aug-cc-pCVQZ	1.087	1.078	2.236	1.284	92.6	828	1.077	1.274	1823

[a]FC and AE denote frozen-core and all-electron computations, respectively.
[b]Dissociation energy (D_e) of (CH_3–HCl) and the vibrationless enthalpy of the reaction (ΔE_e) are given in cm^{-1}.

TABLE III. Focal-point analysis of the classical barrier height (V_{SP}, cm^{-1}) of the $Cl(^2P_{3/2}) + CH_4 \rightarrow HCl + CH_3$ reaction.[a]

	V_{SP}[ROHF]	δ[RMP2]	δ[UCCSD]	δ[UCCSD(T)]	δ[UCCSDT]	δ[UCCSDT(Q)]	V_{SP}
aug-cc-pVDZ	7917	−5430	+981	−642	−29	−54	2744
aug-cc-pVTZ	8095	−5826	+1285	−843	+16	[−54]	2673
aug-cc-pVQZ	8086	−6024	+1321	−875	[+16]	[−54]	2470
aug-cc-pV5Z	8045	−6089	+1354	−890	[+16]	[−54]	2382
aug-cc-pV6Z	8039	−6077	+1359	[−890]	[+16]	[−54]	2394
CBS[b]	8038	−6059	+1366	−906	+16	−54	**2402**

$V_{SP}(\text{final}) = V_{SP}(\text{FC-UCCSDT(Q)/CBS}) + \Delta_{Core} + \Delta_{Rel.} + \Delta_{SO} = 2402 - 21 - 6 + 294 = \mathbf{2669}$

[a]The results correspond to the structures optimized at the all-electron UCCSD(T)/aug-cc-pCVTZ level of theory. The symbol δ denotes the increments in V_{SP} with respect to the preceding level of theory. Brackets signify assumed, non-extrapolated, increments from smaller basis set results. Previously published as Table S2 of Ref. 18. The bold numbers are the final FPA results with and without small corrections (core, relativistic, and SO).

[b]The complete basis set (CBS) ROHF energy and the RMP2, UCCSD, and UCCSD(T) electron correlation energies were calculated using two-parameter extrapolation formulae given in Eqs. (1) and (2), respectively. Only the best two energies were included in the extrapolations.

and scalar relativistic effects are small, −21 and −6 cm^{-1}, respectively. However, the SO effect is significant, since it effectively increases the barrier by 294 cm^{-1}. We took all the above effects into account; thus, we arrived to the new benchmark value for the classical barrier height (2670 ± 40 cm^{-1}). (Note that a recent study[28] reported a classical barrier height of 2385 cm^{-1} obtained at CCSD(T)/CBS//CCSD(T)/aug-cc-pVTZ, which value is slightly smaller than our more rigorous CCSD(T)/CBS value of 2440 cm^{-1} and much smaller than our benchmark value of 2670 cm^{-1}. The difference in the CBS value is due to the fact that Ref. 28 extrapolates from TZ and QZ results, whereas we use more accurate 5Z and 6Z energies to determine the CBS limit. The main reason of the large difference between the final benchmark values is that Ref. 28 neglects the SO effect.) Furthermore, applying harmonic zero-point energy (ZPE) correction we get the final vibrationally adiabatic ground state barrier height of 1200 ± 200 cm^{-1}, whose larger estimated uncertainty is due to the uncertainty of the ZPE correction, especially the effect of the vibrational anharmonicity.

The well in the product channel, of C_{3v} symmetry, has equilibrium C–H_b and H_b–Cl distances of 2.236 and 1.284 Å, respectively, obtained at the AE-UCCSD(T)/aug-cc-pCVQZ level of theory. The latter is just slightly longer than the bond length of the HCl molecule (1.274 Å). As Table IV shows, the FPA analysis of the D_e is well converged; the post-UCCSD(T) correlation effect is only +5 cm^{-1}. The aug-cc-pV*X*Z bases with X = D, T, Q, 5, and 6 overestimate the D_e by 134, 87, 46, 26, and 13 cm^{-1}, respectively, relative to the CBS limit. After applying the minor correction for core electron correlation (+9 cm^{-1}) and the scalar relativistic effect (+14 cm^{-1}), the final accurate D_e is 820 ± 10 cm^{-1}. We expect this relatively deep well to affect the product state distributions, especially the rotational and angular distributions. In Fig. 3 the variation of the potential of this well is shown as a function of the C–Cl–H_b angle keeping all other coordinates fixed at their equilibrium values. As seen, there is a fairly steep dependence on this angle, indicating a significant orienting force for the collinear C–H_b–Cl configuration. More discussion of the dynamical effects of this hindering is given in Sec. IV. Also, because this well is much deeper than the entrance channel one, it is of interest to investigate whether it supports a bound state. We estimate this using the harmonic ZPE. Based on that, we estimate D_0 to be 350 ± 50 cm^{-1}. We do not report a similar harmonic analysis for the entrance channel well because the motion in that shallower well is likely much more anharmonic than the exit channel one. Thus, we believe that a harmonic analysis of whether there is a bound state in the

TABLE IV. Focal-point analysis of the dissociation energy (D_e, cm^{-1}) of the exit-channel complex (CH_3–HCl).[a]

	D_e[ROHF]	δ[RMP2]	δ[UCCSD]	δ[UCCSD(T)]	δ[UCCSDT]	δ[UCCSDT(Q)]	D_e
aug-cc-pVDZ	18	+948	−164	+120	+4	+6	932
aug-cc-pVTZ	−39	+974	−196	+140	−1	[+6]	885
aug-cc-pVQZ	−61	+962	−207	+144	[−1]	[+6]	844
aug-cc-pV5Z	−74	+957	−210	+145	[−1]	[+6]	824
aug-cc-pV6Z	−78	+946	−208	[+145]	[−1]	[+6]	811
CBS[b]	−78	+931	−206	+146	−1	+6	**798**

$D_e(\text{final}) = D_e(\text{FC-UCCSDT(Q)/CBS}) + \Delta_{Core} + \Delta_{Rel.} + \Delta_{SO} = 798 + 9 + 14 + 0 = \mathbf{821}$

[a]The results correspond to the structures optimized at the all-electron UCCSD(T)/aug-cc-pCVQZ level of theory. The symbol δ denotes the increments in D_e with respect to the preceding level of theory. Brackets signify assumed, non-extrapolated, increments from smaller basis set results. The final FPA result was previously published in Ref. 18. The bold numbers are the final FPA results with and without small corrections (core, relativistic, and SO).

[b]The complete basis set (CBS) ROHF energy and the RMP2, UCCSD, and UCCSD(T) electron correlation energies were calculated using two-parameter extrapolation formulae given in Eqs. (1) and (2), respectively. Only the best two energies were included in the extrapolations.

TABLE V. Focal-point analysis of the vibrationless endoergicity (ΔE_e, cm^{-1}) of the $Cl(^2P_{3/2}) + CH_4 \rightarrow HCl + CH_3$ reaction.[a]

	ΔE_e[ROHF]	δ[RMP2]	δ[UCCSD]	δ[UCCSD(T)]	δ[UCCSDT]	δ[UCCSDT(Q)]	ΔE_e
aug-cc-pVDZ	3032	−748	+244	−89	−5	−20	2414
aug-cc-pVTZ	2795	−837	+439	−149	+18	−26	2240
aug-cc-pVQZ	2691	−980	+409	−156	[+18]	[−26]	1956
aug-cc-pV5Z	2577	−1029	+416	−163	[+18]	[−26]	1794
aug-cc-pV6Z	2556	−1021	+413	−164	[+18]	[−26]	1776
CBS[b]	2551	−1010	+408	−166	+18	−26	**1775**

$\Delta E_e(\text{final}) = \Delta E_e(\text{FC-UCCSDT(Q)/CBS}) + \Delta_{\text{Core}} + \Delta_{\text{Rel.}} + \Delta_{\text{SO}} = 1775 - 18 + 40 + 294 = \mathbf{2091}$

[a]The results correspond to the structures optimized at the all-electron UCCSD(T)/aug-cc-pCVQZ level of theory. The symbol δ denotes the increments in ΔE_e with respect to the preceding level of theory. Brackets signify assumed, non-extrapolated, increments from smaller basis set results. The final FPA result was previously published in Ref. 18. The bold numbers are the final FPA results with and without small corrections (core, relativistic, and SO).

[b]The complete basis set (CBS) ROHF energy and the RMP2, UCCSD, and UCCSD(T), electron correlation energies were calculated using two-parameter extrapolation formulae given in Eqs. (1) and (2), respectively. Only the best two energies were included in the extrapolations.

shallow entrance channel well would be too unreliable to report.

The abstraction reaction endoergicity is 2090 ± 20 cm^{-1} relative to $Cl(^2P_{3/2}) + CH_4(eq)$. In order to achieve this high accuracy, significant basis set effects as well as the SO correction were taken into account. The aug-cc-pV*X*Z bases with X = D, T, Q, 5, and 6 overestimate the reaction endoergicity by 639, 465, 181, 19, and 1 cm^{-1}, respectively, relative to the CBS limit. This shows good convergence to the CBS limit; however, it is important to note the poor performance of the DZ and TZ (even QZ if high accuracy is aimed) bases. The SO correction has an effect of +294 cm^{-1} on the endoergicity. Furthermore, the scalar relativistic effect is also not negligible, since it is +40 cm^{-1}. If we take the significant anharmonic ZPE correction (−1730 cm^{-1}) into account, we arrive at the final 0 K reaction enthalpy of 360 ± 30 cm^{-1}. (Note that the harmonic ZPE correction (−1820 cm^{-1}) gives a reaction enthalpy of 270 cm^{-1}.) The experimental reaction enthalpy, obtained from the 0 K enthalpies of formation of the reactants and products taken from the NIST database, is 410 ± 40 cm^{-1}, which is in good agreement with the above computed benchmark value.

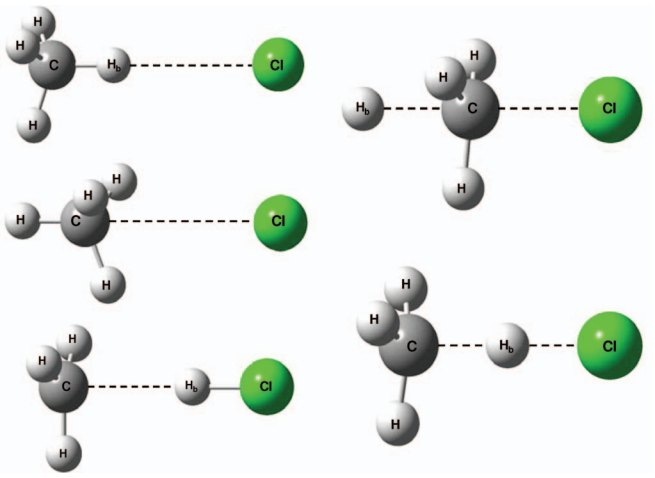

FIG. 2. Structures of the entrance- and exit-channel complexes (left) and saddle points (right). All the structures have C_{3v} point-group symmetry.

D. The Cl + CH_4 → H + CH_3Cl reaction

The structures of the first-order saddle point $(H_b–CH_3–Cl)_{SP}$ (see Fig. 2) and the reactant and product molecules computed at different levels of theory are given in Table VI. The benchmark FPA results for the classical barrier height and reaction endoergicity are given in Tables VII and VIII, respectively.

At the saddle point the C–H_b distance is 1.540 Å, i.e., significantly stretched relative to the CH bond length of CH_4 (1.087 Å). The C–Cl distance (2.014 Å) is longer by 0.230 Å than that of the CH_3Cl product. The saddle-point structure is already inverted, since the α(H–C–Cl) bond angle is 97.0°, i.e., larger than 90°, though less than the same bond angle in CH_3Cl (108.4°). The classical barrier height for the substitution reaction is $14\,720 \pm 80$ cm^{-1}, a much higher barrier than that of the abstraction reaction. The basis set effect on

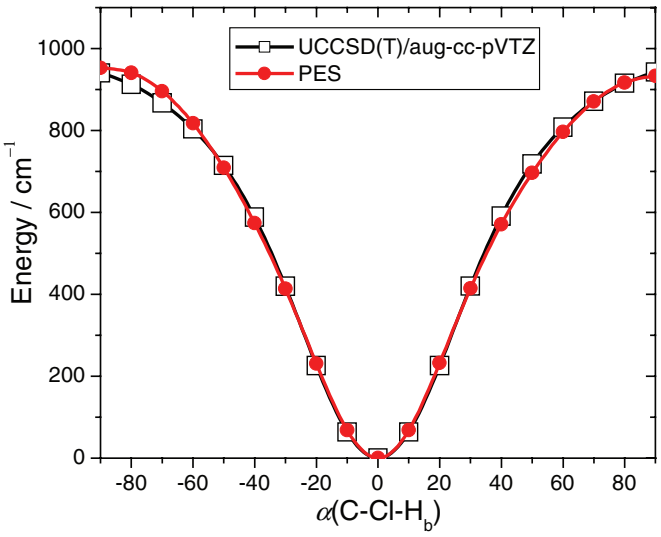

FIG. 3. Potential energy curves for $(CH_3–H_bCl)$ as a function of the C–Cl–H_b angle computed at the UCCSD(T)/aug-cc-pVTZ level of theory and obtained from the PES. The minimum corresponds to the equilibrium structure of $(CH_3–HCl)$ shown in Fig. 2. Bending of the C–Cl–H_b angle was done in the C_s plane keeping all the other coordinates fixed at their equilibrium values. Negative and positive angles correspond to configurations where the two H atoms in the C_s plane are in "trans" and "cis" positions, respectively.

TABLE VI. Structures (in Å and degrees) of the reactant, product, and the saddle point $(H_b–CH_3–Cl)_{SP}$ as well as classical barrier height and reaction endoergicity at different levels of theory for the $Cl(^2P) + CH_4 \rightarrow H + CH_3Cl$ reaction.[a]

	Cl + CH_4	$(H–CH_3–Cl)_{SP}$ (C_{3v})					H + CH_3Cl (C_{3v})			
Methods[a]	r(CH)	r(CH)	$r(CH_b)$	r(CCl)	α(HCCl)	V_{SP}[b]	r(CH)	r(CCl)	α(HCCl)	ΔE_e[b]
FC-UMP2/aug-cc-pVDZ	1.098	1.092	1.488	2.021	96.2	1 5304	1.096	1.797	108.2	7732
FC-UMP2/aug-cc-pVTZ	1.086	1.081	1.471	2.002	96.2	14 857	1.084	1.780	108.4	7181
FC-UMP2/aug-cc-pVQZ	1.085	1.080	1.464	1.996	96.1	14 587	1.083	1.775	108.5	6816
AE-UMP2/aug-cc-pCVDZ	1.097	1.091	1.485	2.018	96.1	15 090	1.095	1.793	108.3	7468
AE-UMP2/aug-cc-pCVTZ	1.085	1.079	1.465	1.996	96.1	14 677	1.083	1.772	108.5	6845
AE-UMP2/aug-cc-pCVQZ	1.083	1.078	1.460	1.991	96.1	14 477	1.081	1.767	108.6	6571
FC-UCCSD(T)/aug-cc-pVDZ	1.103	1.095	1.565	2.040	97.0	15 400	1.100	1.809	108.1	9614
FC-UCCSD(T)/aug-cc-pVTZ	1.090	1.083	1.546	2.020	97.1	14 973	1.087	1.792	108.2	9183
FC-UCCSD(T)/aug-cc-pVQZ	1.088						1.085	1.786	108.3	8783
AE-UCCSD(T)/aug-cc-pCVDZ	1.101	1.094	1.561	2.036	97.0	15 253	1.098	1.805	108.1	9414
AE-UCCSD(T)/aug-cc-pCVTZ	1.088	1.081	1.540	2.014	97.0	14 900	1.085	1.784	108.3	8947
AE-UCCSD(T)/aug-cc-pCVQZ	1.087						1.084	1.779	108.4	8648

[a]FC and AE denote frozen-core and all-electron computations, respectively.
[b]Classical barrier height (V_{SP}) and the vibrationless enthalpy of the reaction (ΔE_e) are given in cm^{-1}.

the barrier height is significant, since the aug-cc-pV*X*Z bases with X = D, T, Q, 5, and 6 give too high barrier by 854, 475, 185, 52, and 41 cm^{-1}, respectively, relative to the CBS limit. Furthermore, the post-UCCSD(T) electron correlation effects are also significant, i.e., lower the barrier by about 100 cm^{-1}. As for all the other energies relative to Cl + CH_4, the SO effect increases the barrier by 294 cm^{-1}. The harmonic ZPE correction lowers the barrier by 1134 cm^{-1}; thus, the vibrationally adiabatic ground state barrier height is 13 590 ± 120 cm^{-1}.

The benchmark endoergicity of the substitution reaction is 8810 ± 50 cm^{-1}, which is much higher than that of the abstraction reaction. The harmonic ZPE correction decreases the endoergicity by 1515 cm^{-1}; thus, the 0 K reaction enthalpy is 7300 ± 100 cm^{-1} (the accuracy could be improved by applying anharmonic ZPE correction). The experimental value (0 K) based on the NIST database is 7450 ± 60 cm^{-1} indicating that the harmonic ZPE correction is too large, as expected. One has to employ at least the UCCSD(T) method to get accurate endoergicity, since ROHF overestimates by 1175 cm^{-1}, UMP2 underestimates by 1687 cm^{-1}, and UCCSD overestimates by 810 cm^{-1} relative to UCCSDT(Q). The error of UCCSD(T) relative to UCCSDT(Q) is only 22 cm^{-1}, which is a good example why the UCCSD(T) is called the "gold standard" of electronic structure theory. As shown in many cases before, large basis sets are needed for quantitative accuracy, since the aug-cc-pV*X*Z bases overestimate the endoergicity by 1135, 706, 298, 80, and 47 cm^{-1}, for X = D, T, Q, 5, and 6, respectively. The core electron correlation correction (−28 cm^{-1}) and scalar relativistic effect (+34 cm^{-1}) almost cancel each other, whereas the SO correction, again, increases the reaction endoergicity by 294 cm^{-1}.

The summary of the FPA analysis for both reaction channels is given in Table IX and a schematic of the global PES showing the stationary points and the benchmark energetics is given in Fig. 4. In order to achieve the high accuracy of the above-described relative energies it was essential to employ large basis sets (in many cases even the aug-cc-pVQZ basis was found not large enough) and extrapolations to the CBS limit. Note that the uncertainty of the CBS extrapolation significantly decreases if one uses large basis set data

TABLE VII. Focal-point analysis of the classical barrier height (V_{SP}, cm^{-1}) of the $Cl(^2P_{3/2}) + CH_4 \rightarrow H + CH_3Cl$ reaction.[a]

	V_{SP}[ROHF]	δ[RMP2]	δ[UCCSD]	δ[UCCSD(T)]	δ[UCCSDT]	δ[UCCSDT(Q)]	V_{SP}
aug-cc-pVDZ	21 595	−6120	+1044	−1107	−74	−94	15 246
aug-cc-pVTZ	21 718	−6653	+1325	−1415	−14	[−94]	14 867
aug-cc-pVQZ	21 735	−6935	+1356	−1472	[−14]	[−94]	14 577
aug-cc-pV5Z	21 708	−7056	+1399	−1499	[−14]	[−94]	14 444
aug-cc-pV6Z	21 706	−7082	+1416	[−1499]	[−14]	[−94]	14 433
CBS[b]	21 705	−7118	+1440	−1528	−14	−94	**14 392**

$$V_{SP}(\text{final}) = V_{SP}(\text{FC-UCCSDT(Q)/CBS}) + \Delta_{Core} + \Delta_{Rel.} + \Delta_{SO} = 14\,392 + 40 - 7 + 294 = \mathbf{14\,719}$$

[a]The results correspond to the structures optimized at the all-electron UCCSD(T)/aug-cc-pCVTZ level of theory. The symbol δ denotes the increments in V_{SP} with respect to the preceding level of theory. Brackets signify assumed, non-extrapolated, increments from smaller basis set results. The final FPA result was previously published in Ref. 18. The bold numbers are the final FPA results with and without small corrections (core, relativistic, and SO).
[b]The complete basis set (CBS) ROHF energy and the RMP2, UCCSD, and UCCSD(T) electron correlation energies were calculated using two-parameter extrapolation formulae given in Eqs. (1) and (2), respectively. Only the best two energies were included in the extrapolations.

TABLE VIII. Focal-point analysis of the vibrationless endoergicity (ΔE_e, cm^{-1}) of the $Cl(^2P_{3/2}) + CH_4 \rightarrow H + CH_3Cl$ reaction.[a]

	ΔE_e[ROHF]	δ[RMP2]	δ[UCCSD]	δ[UCCSD(T)]	δ[UCCSDT]	δ[UCCSDT(Q)]	ΔE_e
aug-cc-pVDZ	10 225	−2307	+2291	−554	+44	−54	9646
aug-cc-pVTZ	9912	−2504	+2536	−750	+98	−76	9217
aug-cc-pVQZ	9806	−2725	+2497	−791	[+98]	[−76]	8809
aug-cc-pV5Z	9707	−2828	+2501	−811	[+98]	[−76]	8591
aug-cc-pV6Z	9689	−2842	+2499	[−811]	[+98]	[−76]	8558
CBS[b]	9686	−2861	+2497	−833	+98	−76	**8511**

$$\Delta E_e(\text{final}) = \Delta E_e(\text{FC-UCCSDT(Q)/CBS}) + \Delta_{\text{Core}} + \Delta_{\text{Rel.}} + \Delta_{\text{SO}} = 8511 - 28 + 34 + 294 = \mathbf{8811}$$

[a]The results correspond to the structures optimized at the all-electron UCCSD(T)/aug-cc-pCVQZ level of theory. The symbol δ denotes the increments in ΔE_e with respect to the preceding level of theory. Brackets signify assumed, non-extrapolated, increments from smaller basis set results. The final FPA result was previously published in Ref. 18. The bold numbers are the final FPA results with and without small corrections (core, relativistic, and SO).

[b]The complete basis set (CBS) ROHF energy and the RMP2, UCCSD, and UCCSD(T) electron correlation energies were calculated using two-parameter extrapolation formulae given in Eqs. (1) and (2), respectively. Only the best two energies were included in the extrapolations.

($X = 5$ and 6 in the present study). The post-UCCSD(T) electron correlation effect was the largest on the barrier height of the substitution reaction, although it decreases the barrier by only 1%, since the barrier height is a large value. The SO energy shift of the reactant asymptote cannot be neglected since it is larger than the uncertainty of the present benchmark FPA study.

III. GLOBAL *AB INITIO* POTENTIAL ENERGY SURFACE

The analytical full-dimensional PES is a permutationally invariant fit to high-quality *ab initio* energy points. We present below the details of the *ab initio* computations and the fit and then we show the accuracy of the PES by comparing to the new benchmark data described in Sec. II.

A. The *ab initio* data

The accuracy of the *ab initio* energy points determines the quality of the PES; therefore, it is important to use an electronic structure method that gives reasonably accurate energies. However, one also needs to consider the computational cost, since a global fit usually requires more than 10 000 data points, whose high-level computations can be very time consuming. In order to achieve the best accuracy with affordable

TABLE IX. Summary of the focal-point analysis results (in cm^{-1}) including the effects of the core electron correlation (Core), scalar relativity (Rel.), the spin-orbit (SO) couplings, and zero-point vibrational energy (ZPE) for the barrier heights and enthalpies of the $Cl + CH_4 \rightarrow HCl + CH_3$ and $H + CH_3Cl$ reactions as well as for the dissociation energy of (CH_3–HCl).

	$Cl + CH_4 \rightarrow HCl + CH_3$			$Cl + CH_4 \rightarrow H + CH_3Cl$	
	Barrier height[a]	Dissociation energy[b]	Reaction enthalpy[b]	Barrier height[a]	Reaction enthalpy[b]
ROHF[c]	8038	− 78	2551	21 705	9686
RMP2[c]	1979	853	1541	14 588	6824
UCCSD[c]	3345	646	1949	16 028	9321
UCCSD(T)[c]	2440	792	1783	14 500	8489
UCCSDT[c]	2455	792	1801	14 486	8586
UCCSDT(Q)[c]	2402	798	1775	14 392	8511
ΔCore[d]	− 21	+9	− 18	+40	− 28
ΔRel.[e]	− 6	+14	+40	− 7	+34
ΔSO[f]	+294	+0	+294	+294	+294
Final classical[g]	**2669**	**821**	**2091**	**14 719**	**8811**
ΔZPE[h]	− 1471	− 474	− 1820 (− 1730)	− 1134	− 1515
Final + ΔZPE	**1198**	**347**	**271 (361)**	**13 585**	**7296**

[a]The results correspond to the structures optimized at the all-electron (AE) UCCSD(T)/aug-cc-pCVTZ level of theory.

[b]The results correspond to the structures optimized at the AE-UCCSD(T)/aug-cc-pCVQZ level of theory.

[c]The results correspond to the complete basis set limit (see Tables III–V and VII and VIII).

[d]Core-core and core-valence correlation effects obtained as the difference between all-electron and frozen-core energies at the UCCSD(T)/aug-cc-pCVQZ level of theory.

[e]Douglas–Kroll relativistic corrections computed at the AE-UCCSD(T)/aug-cc-pCVQZ level of theory.

[f]Spin-orbit corrections obtained from the experimental Cl atom splitting ($\varepsilon = 882\ cm^{-1}$), as $\varepsilon/3 = 294\ cm^{-1}$.

[g]The final classical results were previously reported in Ref. 18.

[h]Harmonic zero-point vibrational energy (ZPE) corrections obtained at the UCCSD(T)/aug-cc-pVTZ level of theory. In parenthesis the variationally computed anharmonic ZPE correction is given.

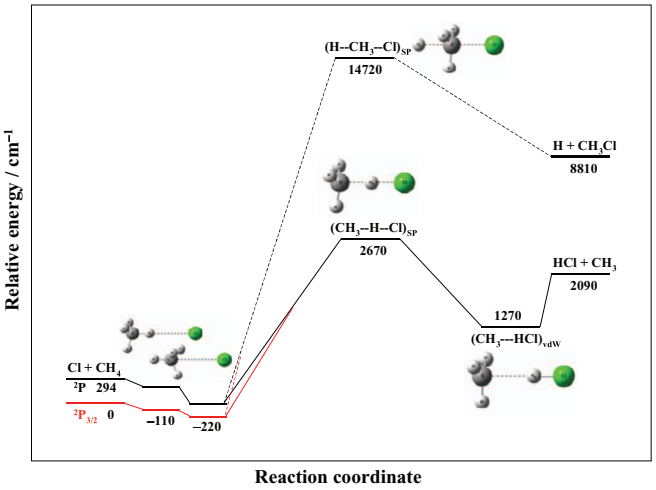

FIG. 4. Schematics of the global spin-orbit (SO) and non-SO potential energy surfaces of the Cl + CH_4 reaction showing the benchmark electronic energies relative to Cl($^2P_{3/2}$) + CH_4(eq). The figure is adapted from Fig. 1 in Ref. 18.

computational time, we used a composite approach, where the energies are defined as

$$E\left[\frac{\text{UCCSD(T)}}{\text{aug-cc-pVDZ}}\right] + E\left[\frac{\text{AE-UMP2}}{\text{aug-cc-pCVTZ}}\right] - E\left[\frac{\text{UMP2}}{\text{aug-cc-pVDZ}}\right]. \quad (3)$$

In Table X we present results testing the performance of this composite method. For 15 configurations with energies up to 13 000 cm^{-1} above Cl + CH_4(eq) we found that this composite method gives AE-CCSD(T)/aug-cc-pCVQZ high-quality results with an RMS of only 130 cm^{-1}, whereas the RMS errors of CCSD(T) with the aug-cc-pVDZ and aug-cc-pVTZ bases are 1260 and 390 cm^{-1}, respectively (for more details see Table X). Furthermore, the composite method reduces the computational time by factors of about 1000 and 5 relative to AE-CCSD(T)/aug-cc-pCVQZ and CCSD(T)/aug-cc-pVTZ, respectively. These test results indicate that the present composite approach outperforms CCSD(T)/aug-cc-pVTZ, which is usually referred to as "high" or "benchmark" level of theory in papers on Cl + CH_4. (We successfully applied a similar composite method to the F + CH_4 reaction,[8] which used FC-UMP2/aug-cc-pVTZ instead of AE-UMP2/aug-cc-pCVTZ in Eq. (3). The method used for F + CH_4 is computationally slightly less expensive, but gives a RMS of 335 cm^{-1} for the Cl + CH_4 reaction, whereas Eq. (3) gives RMS of only 130 cm^{-1}.)

As mentioned in Sec. II, the SO interaction plays an important role in the entrance channel, since it effectively increases the barrier height and the reaction endoergicity by 294 cm^{-1} and has a significant effect on the entrance channel vdW well. In order to account for the SO effect, differences between the SO and non-SO ground state electronic energies obtained by MRCI + Q/aug-cc-pVTZ were added to the composite non-SO energies at 1598 $ClCH_4$ configurations in the entrance channel. The 1598 configurations were selected from the total set of configurations based on the following geometrical requirements:

$$r(\text{C} - \text{Cl}) > 2.4\ \text{Å} \quad \text{and} \quad \min[r(\text{H} - \text{Cl})] > 1.8\ \text{Å} \quad \text{and} \quad \max[r(\text{C} - \text{H})] < 1.3\ \text{Å}. \quad (4)$$

Furthermore, 2000 Cl + CH_4 fragment data were also shifted by the constant SO correction of the Cl atom. The SO

TABLE X. Test of the composite method employed for the CH_4Cl system at different regions (along the H_3C–H_b–Cl C_{3v} axis) of the global potential energy surface.

r(CH)[a]	r(CH_b)[a]	r(H_bCl)[a]	α(HCH_b)[a]	Δ[MP2/aVDZ][b]	Δ[AE-MP2/aCVTZ][b]	Δ[CCSD(T)/aVDZ][b]	Δ[CCSD(T)/aVTZ][b]	Δ[AE-CCSD(T)/aCVTZ][b]	Δ[AE-Composite][b]	AE-CCSD(T)/aCVQZ[b]
1.087	1.087	∞	109.5	0	0	0	0	0	0	0
1.100	1.100	2.500	109.5	−183	−14	−300	−83	−84	−130	**−4**
1.100	1.100	2.000	110.0	+102	+31	−62	−38	−66	−132	**577**
1.100	3.000	1.300	90.0	−62	−218	+92	+317	+152	−65	**1632**
1.100	1.800	1.300	90.0	+42	−352	+308	+324	+131	−86	**1814**
1.084	1.300	1.500	105.0	+356	+14	+321	+210	+95	−21	**2403**
1.084	1.407	1.443	101.0	+245	−107	+330	+253	+125	−23	**2453**
1.084	1.200	1.400	100.0	+442	−321	+759	+362	+148	−4	**4277**
1.100	2.000	1.500	90.0	−294	−55	−299	+167	+128	−60	**4798**
1.200	1.300	1.500	105.0	−461	+276	−941	−44	−44	−204	**7020**
1.100	2.500	1.100	100.0	+1119	−395	+1459	+617	+179	−55	**7397**
1.000	1.800	1.500	100.0	+1136	−203	+1496	+441	+277	+157	**7430**
1.000	1.200	1.400	100.0	+1587	−412	+2184	+615	+294	+185	**7580**
1.200	1.200	1.400	100.0	−336	−50	−474	+109	+6	−187	**9050**
1.000	2.500	1.100	100.0	+2426	−600	+3196	+911	+349	+170	**10 429**
1.200	2.000	1.600	90.0	−789	+550	−1525	−92	+7	−186	**12 715**
RMS error				**910**	**305**	**1261**	**390**	**170**	**130**	

[a]All the bond lengths (r) are in Å and the bond angles (α) are in degrees.

[b]Δ[MP2/aVDZ], Δ[AE-MP2/aCVTZ], Δ[CCSD(T)/aVDZ], Δ[CCSD(T)/aVTZ], Δ[AE-CCSD(T)/aCVTZ], and Δ[AE-composite] denote the deviations (in cm^{-1}) from the corresponding AE-CCSD(T)/aCVQZ relative energy, where AE-composite = CCSD(T)/aVDZ + AE-MP2/aCVTZ − MP2/aVDZ and AE means all-electron computations (for more details see Sec. III). All the energies are relative to the same reference configuration, which is the reactant, i.e., Cl + CH_4, asymptote.

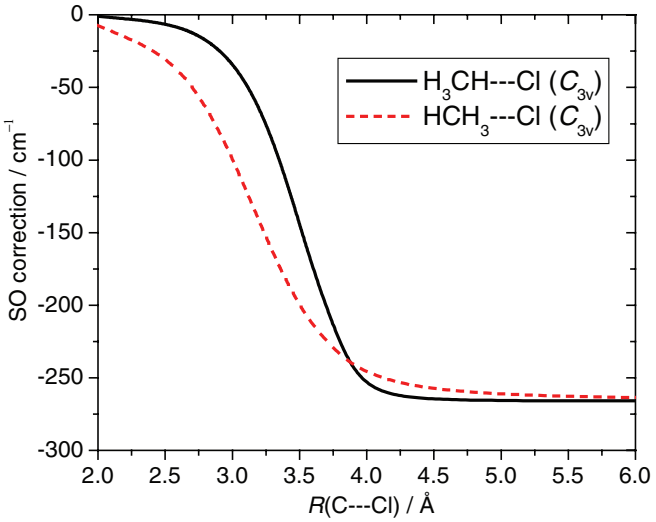

FIG. 5. Spin-orbit correction curves of CH_4–Cl as a function of the C–Cl distance along the C_{3v} axis with fixed CH_4(eq) geometry and CH–Cl and HC–Cl linear bond arrangements obtained as energy difference between the non-SO and SO ground state potentials computed at the MRCI + Q/aug-cc-pVTZ level of theory.

corrections as a function of the C–Cl distance are shown in Fig. 5 for the CH–Cl and HC–Cl linear bond arrangements. As seen, the absolute SO corrections start to decrease from the asymptotic atomic limit at about 4 Å and the effect almost vanishes around a 2 Å C–Cl distance. Figure 5 also shows that SO correction depends on the orientation of CH_4 and the effect is larger at HC–Cl configurations than at CH–Cl.

Finally, since there is significant BSSE in the entrance channel, which affects the depth of the vdW well (see Fig. 1 middle panels), counterpoise corrections were computed at the AE-UMP2/aug-cc-pCVTZ level of theory at the above-mentioned 1598 entrance channel configurations. Note, that these BSSE corrections are almost independent on the method; thus, the BSSEs at UCCSD(T)/aug-cc-pVDZ and UMP2/aug-cc-pVDZ cancel in Eq. (3). This BSSE cancellation in the case of the smaller basis set computations is a nice demonstration of the utility of the composite electronic structure methods. Since the well in the exit channel is much deeper than that in the entrance channel, the relative error caused by BSSE is less significant in the exit well. The basis set dependence as well as the "BSSE-free" CBS limit of the D_e of (CH_3–HCl) is shown in Table IV, indicating an about 10% BSSE for the D_e using the aug-cc-pVTZ basis. Although we did not apply BSSE correction in the exit channel, the PES reproduces the benchmark D_e very well (only 4% deviation) as we show below in Sec. III C.

B. Fitting the *ab initio* energies

The initial dataset included roughly 14 000 configurations in the complex region ($ClCH_4$) as well as 2000, 2000, 2000, and 1000 data points for the fragment channels Cl + CH_4, HCl + CH_3, H_2 + CH_2Cl, and H + CH_3Cl, respectively. We selected these configurations using the F + CH_4 dataset,[8] which was obtained by running low-level direct dynamics computations. Furthermore, the dataset for Cl + CH_4 was augmented with randomly displaced configurations of well-known $ClCH_4$ stationary-point structures. After applying an energy cutoff of 50 000 cm^{-1} the final number of data points was roughly 16 000. The PES was represented by a polynomial expansion in variables $y_{ij} = \exp(-r_{ij}/a)$, where r_{ij} are the inter-atomic distances and a was fixed at 2 bohr, using a polynomial basis that is invariant under permutations of the four identical H atoms. Including all terms up to total degree six, 3262 coefficients were determined by a weighted linear least-squares fit of the above-mentioned 16 000 energy points. In the fit a configuration at energy E relative to the global minimum had weight $E_0/(E + E_0)$, where E_0 = 11 000 cm^{-1}. The RMS fitting errors are 72, 128, and 347 cm^{-1} for energy intervals (0, 11 000), (11 000, 22 000), and (22 000, 50 000) cm^{-1}, respectively. Note that the RMS fitting error up to 22 000 cm^{-1} is below the expected accuracy of the data points (see Table X); thus, the fit does not compromise the accuracy of the PES. We carried out two fits, one to the non-SO data points and another to the SO-corrected *ab initio* data. As a result, we obtained the PESs for the

TABLE XI. Properties of the global potential energy surface (PES) for the Cl + CH_4 → HCl + CH_3 reaction. (Previously published as Table S1 of Ref. 18.)

Cl + CH_4				(CH_3–H_b–Cl)$_{SP}$				(CH_3–HCl)				HCl + CH_3			
	PES[a]	aVTZ[b]	Acc.[c]		PES[a]	aVTZ[b]	Acc.[c]		PES[a]	aVTZ[b]	Acc.[c]		PES[a]	aVTZ[b]	Acc.[c]
Structures[d]															
r(CH)	1.089	1.090	1.087	r(CH)	1.083	1.084	1.083	r(CH)	1.080	1.081	1.078	r(CH)	1.079	1.080	1.077
				r(CH_b)	1.403	1.407	1.397	r(CH_b)	2.274	2.223	2.236				
				r(H_bCl)	1.437	1.443	1.443	r(H_bCl)	1.282	1.289	1.284	r(HCl)	1.276	1.279	1.274
				α(HCH_b)	101.0	101.0	101.1	α(HCH_b)	92.8	93.0	92.6				
Relative energies (cm^{-1})															
Non-SO	0	0	0	Non-SO	2384	2711	2375	Non-SO	892	1367	976	Non-SO	1751	2247	1797
SO	0	0	0	SO	2648	3005[e]	2669[e]	SO	1156	1661[e]	1270[e]	SO	2010	2541[e]	2091[e]

[a]Results corresponding to the non-SO and SO PESs. The two PESs give the same structural parameters within 0.001 Å and 0.1°, except for CH_b (CH_3–HCl), where the SO PES value is reported in the table and the non-SO PES gives 2.276 Å.

[b]Results obtained by *ab initio* calculations at the frozen-core UCCSD(T)/aug-cc-pVTZ level of theory.

[c]Accurate structures obtained at all-electron UCCSD(T)/aug-cc-pCVTZ [(CH_3–H_b–Cl)$_{SP}$] and all-electron UCCSD(T)/aug-cc-pCVQZ [all the other species] levels of theory. The highly accurate relative energies were obtained from the focal-point analysis as given in Table IX.

[d]All the bond lengths (r) are in Å and the bond angles (α) are in degrees. See Fig. 2 for the notations.

[e]The SO energy shift is obtained from the experimental Cl atom splitting (ε = 882 cm^{-1}), as $\varepsilon/3$ = 294 cm^{-1}.

TABLE XII. Properties of the global potential energy surface (PES) for the Cl + CH_4 → H + CH_3Cl reaction.

Cl + CH_4				$(H_b–CH_3–Cl)_{SP}$				H + CH_3Cl			
	PES[a]	aVTZ[b]	Acc.[c]		PES[a]	aVTZ[b]	Acc.[c]		PES[a]	aVTZ[b]	Acc.[c]
Structures[d]											
r(CH)	1.089	1.090	1.087	r(CH)	1.083	1.083	1.081	r(CH)	1.085	1.087	1.084
				$r(CH_b)$	1.532	1.546	1.540				
				r(CCl)	2.015	2.020	2.014	r(CCl)	1.790	1.792	1.779
				α(HCCl)	97.8	97.1	97.0	α(HCCl)	108.7	108.2	108.4
Relative energies (cm^{-1})											
Non-SO	0	0	0	Non-SO	14 795	14 973	14 425	Non-SO	8840	9183	8517
SO	0	0	0	SO	15 061	15 267[e]	14 719[e]	SO	9087	9477[e]	8811[e]

[a]Results corresponding to the non-SO and SO PESs. The two PESs give the same structural parameters within 0.001 Å and 0.1°.
[b]Results obtained by *ab initio* calculations at the frozen-core UCCSD(T)/aug-cc-pVTZ level of theory.
[c]Accurate structures obtained at all-electron UCCSD(T)/aug-cc-pCVTZ [$(H_b–CH_3–Cl)_{SP}$] and all-electron UCCSD(T)/aug-cc-pCVQZ [CH_4 and CH_3Cl] levels of theory. The highly accurate relative energies were obtained from the focal-point analysis as given in Table IX.
[d]All the bond lengths (r) are in Å and the bond angles (α) are in degrees. See Fig. 2 for the notations.
[e]The SO energy shift is obtained from the experimental Cl atom splitting ($\varepsilon = 882\ cm^{-1}$), as $\varepsilon/3 = 294\ cm^{-1}$.

non-SO and SO ground electronic states of the Cl + CH_4 reaction, hereafter we denote these PESs as non-SO PES and SO PES, respectively. We gave the RMS errors for the SO PES above; the RMS values for the non-SO PES are the same within 5 cm^{-1}.

C. The accuracy of the potential energy surface

Properties of the global PES and their comparison to new benchmark *ab initio* data are given in Tables XI and XII for the abstraction and substitution reactions, respectively. As seen, the structures obtained from optimization on the PES are often more accurate than those obtained from direct CCSD(T)/aug-cc-pVTZ computations, compared to high-level *ab initio* data (AE-CCSD(T)/aug-cc-pCVTZ and AE-CCSD(T)/aug-cc-pCVQZ for the saddle points and minima, respectively). For the abstraction reaction the SO PES has a classical barrier height, D_e for (CH_3–HCl), and endoergicity of 2648, 854, and 2010 cm^{-1}, respectively. The corresponding benchmark FPA values are 2669, 821, and 2091 cm^{-1}. This agreement between the PES and benchmark values is extremely good, especially considering that the CCSD(T)/aug-cc-pVTZ level of theory, after applying the correct SO shifts, gives energies of 3005, 880, 2541 cm^{-1}, respectively. This shows that even if we use as high level of theory as CCSD(T)/aug-cc-pVTZ we overestimate the barrier height and endoergicity by 336 and 450 cm^{-1}, respectively, whereas the corresponding errors of the PES for these two key energies are only 21 and 81 cm^{-1}. This is the first PES, to our knowledge, that describes the high-energy substitution reaction as well as the abstraction reaction. As Table XII shows, the PES reproduces the substitution barrier height and reaction endoergicity better than the CCSD(T)/aug-cc-pVTZ level of theory and the substitution saddle-point structure is accurate as well.

In Sec. II B we described the benchmark *ab initio* characterization of the entrance channel vdW region and showed the results in Fig. 1. In Fig. 1 we also show the entrance channel potential curves along the C–Cl distance obtained from the non-SO and SO PESs. As seen the agreement between the PES values and the best *ab initio* curves is very good. The PES nicely describes the dependence of the well depth on the orientation of the reactants and the SO effect is also quantitatively described. Figure 1 also reveals the relatively poor accuracy of the CCSD(T)/aug-cc-pVDZ level of theory and shows that the PES is of high accuracy in this region as well.

The harmonic frequencies of the reactant, products, saddle points, and the (CH_3–HCl) complex obtained from the PES and direct *ab initio* computations at CCSD(T) with aug-cc-pVDZ and aug-cc-pVTZ bases are given in Tables XIII–XV. (The differences between the frequencies obtained with the two basis sets indicate the uncertainty of the *ab initio* data.) Note that the composite method used for the PES development [Eq. (3)] is even more accurate than CCSD(T)/aug-cc-pVTZ, as we showed above; thus, we cannot expect exact agreement between the PES and the above mentioned *ab initio* frequencies. Nevertheless, the CCSD(T)/aug-cc-pVTZ frequencies can serve as benchmark data when checking the accuracy of the PES. In contrast

TABLE XIII. Harmonic vibrational frequencies (in cm^{-1}) for CH_4 and $(CH_3–H–Cl)_{SP}$.

CH_4				$(CH_3–H–Cl)_{SP}$			
	PES[a]	aVDZ[b]	aVTZ[b]		PES[a]	aVDZ[b]	aVTZ[b]
ZPE	9818	9738	9833	ZPE	8415	8261	8362
				$\omega(a_1)$	931i	980i	1024i
				$\omega(e)$	345	351	364
				$\omega(a_1)$	499	516	514
				$\omega(e)$	940	885	924
$\omega_4(t_2)$	1355	1319	1351	$\omega(a_1)$	1202	1176	1197
$\omega_2(e)$	1560	1535	1574	$\omega(e)$	1452	1407	1437
$\omega_1(a_1)$	3027	3016	3028	$\omega(a_1)$	3098	3071	3082
$\omega_3(t_2)$	3142	3144	3146	$\omega(e)$	3278	3237	3242

[a]Harmonic frequencies corresponding to the SO-corrected potential energy surface. The non-SO PES gives the same frequencies (the largest deviation is $<2\ cm^{-1}$). Frequencies for CH_4 are taken from Table S3 of Ref. 18.
[b]aVDZ and aVTZ denote *ab initio* results obtained at the UCCSD(T)/aug-cc-pVDZ and UCCSD(T)/aug-cc-pVTZ levels of theory, respectively. aVTZ frequencies for CH_4 are taken from Table S3 of Ref. 18.

TABLE XIV. Harmonic vibrational frequencies (in cm^{-1}) for (CH_3–HCl), CH_3, and HCl.

(CH_3–HCl)				CH_3				HCl			
	PES[a]	aVDZ[b]	aVTZ[b]		PES[a]	aVDZ[b]	aVTZ[b]		PES[a]	aVDZ[b]	aVTZ[b]
ZPE	8517	8441	8487	ZPE	6548	6495	6518	ZPE	1514	1485	1495
$\omega_{HCl}(a_1)$	2880	2841	2834					ω_1	3027	2971	2990
$\omega_s(a_1)$	100	95	101								
$\omega_b(e)$	114	132	136								
$\omega(e)$	345	313	328								
$\omega(a_1)$	643	596	600	$\omega_2(a_2')$	527	497	496				
$\omega(e)$	1412	1404	1419	$\omega_4(e')$	1428	1406	1419				
$\omega(a_1)$	3096	3090	3104	$\omega_1(a_1')$	3128	3101	3114				
$\omega(e)$	3287	3280	3285	$\omega_3(e')$	3293	3290	3294				

[a]Harmonic frequencies corresponding to the SO-corrected potential energy surface. The non-SO PES gives the same frequencies (the largest deviation is <4 cm^{-1}). Frequencies for CH_3 and HCl are taken from Table S3 of Ref. 18.
[b]aVDZ and aVTZ denote *ab initio* results obtained at the UCCSD(T)/aug-cc-pVDZ and UCCSD(T)/aug-cc-pVTZ levels of theory, respectively. aVTZ frequencies for CH_3 and HCl are taken from Table S3 of Ref. 18.

to previous PESs and semi-empirical Hamiltonians[12] which have sizeable errors for some of the frequencies (errors larger than 100 cm^{-1} were not rare), the present PES provides frequencies usually with only a few cm^{-1} deviations from the benchmark *ab initio* results. The interested reader can consult Tables XIII–XV for the detailed data; now we just mention one interesting fundamental. The PES shows that the H–Cl stretching in the (CH_3–HCl) complex is redshifted by 147 cm^{-1} relative to the frequency of the free HCl molecule. The direct *ab initio* CCSD(T)/aug-cc-pVTZ computations provide a redshift of 156 cm^{-1} showing the excellent performance of the PES for a challenging spectroscopic datum.

IV. QUASICLASSICAL TRAJECTORY CALCULATIONS

A. Computational details

QCT calculations of the $Cl(^2P, {}^2P_{3/2}) + CH_4(v = 0) \rightarrow HCl(v, J) + CH_3(n_1n_2n_3n_4)$ and $H + CH_3Cl$ reactions were performed using the global non-SO and SO PESs. We employed standard normal mode sampling[55] and small adjustments to the velocities to prepare the quasiclassical vibrational ground state ($v = 0$ and $J = 0$) of CH_4. The initial distance of the Cl atom from the center of the mass of CH_4 was $\sqrt{x^2 + b^2}$, where b is the impact parameter and x was set to 10 bohr. The orientation of CH_4 was randomly rotated and b was scanned from 0 to 7 bohr with a step size of 0.5 bohr. Five thousand trajectories were computed at each b; thus, the total number of trajectories was 75 000 for each collision energy (E_{coll}). (Note that at $E_{coll} = 1280$ cm^{-1} we increased b with a smaller step size of 0.125 bohr; thus, we computed 285 000 trajectories, because at this E_{coll} detailed experimental rotational distribution data are available.) We have run QCTs at several collision energies in the wide 1050–20 000 cm^{-1} range. All the trajectories were integrated using 0.0726 fs integration step allowing a maximum of 20 000 time steps ($\sim$1.5 ps). (Most of the trajectories finished much faster, i.e., within a few hundred fs.) The trajectories were analyzed with and without any ZPE constraint. Following Ref. 28, the ZPE constrained analysis considers trajectories in which CH_3 or CH_3Cl has at least the corresponding ZPE. We also tested the soft ZPE constraint, which discards trajectories if $E_{vib}(HCl) + E_{vib}(CH_3)$ is less than the sum ZPE(HCl) + ZPE(CH_3) or $E_{vib}(CH_3Cl)$ is less than ZPE(CH_3Cl). We found that this soft ZPE constraint gives similar cross sections and reaction

TABLE XV. Harmonic vibrational frequencies (in cm^{-1}) for CH_4, $(H–CH_3–Cl)_{SP}$, and CH_3Cl.

CH_4				$(H–CH_3–Cl)_{SP}$				CH_3Cl			
	PES[a]	aVDZ[b]	aVTZ[b]		PES[a]	aVDZ[b]	aVTZ[b]		PES[a]	aVDZ[b]	aVTZ[b]
ZPE	9818	9738	9833	ZPE	8803	8600	8699	ZPE	8231	8224	8318
				$\omega(a_1)$	1226*i*	1332*i*	1352*i*				
				$\omega(e)$	410	425	448				
				$\omega(a_1)$	581	557	578	$\omega(a_1)$	730	720	737
				$\omega(e)$	1173	1107	1134	$\omega(e)$	1034	1019	1039
$\omega_4(t_2)$	1355	1319	1351	$\omega(a_1)$	1218	1207	1233	$\omega(a_1)$	1358	1356	1390
$\omega_2(e)$	1560	1535	1574	$\omega(e)$	1427	1396	1417	$\omega(e)$	1502	1461	1500
$\omega_1(a_1)$	3027	3016	3028	$\omega(a_1)$	3169	3076	3086	$\omega(a_1)$	2972	3064	3076
$\omega_3(t_2)$	3142	3144	3146	$\omega(e)$	3309	3253	3251	$\omega(e)$	3165	3174	3178

[a]Harmonic frequencies corresponding to the SO-corrected potential energy surface. The non-SO PES gives basically the same frequencies (the largest deviations are <2, <6, <13 cm^{-1} for CH_4, $(H–CH_3–Cl)_{SP}$, and CH_3Cl, respectively). Frequencies for CH_4 are taken from Table S3 of Ref. 18.
[b]aVDZ and aVTZ denote *ab initio* results obtained at the UCCSD(T)/aug-cc-pVDZ and UCCSD(T)/aug-cc-pVTZ levels of theory, respectively. aVTZ frequencies for CH_4 are taken from Table S3 of Ref. 18.

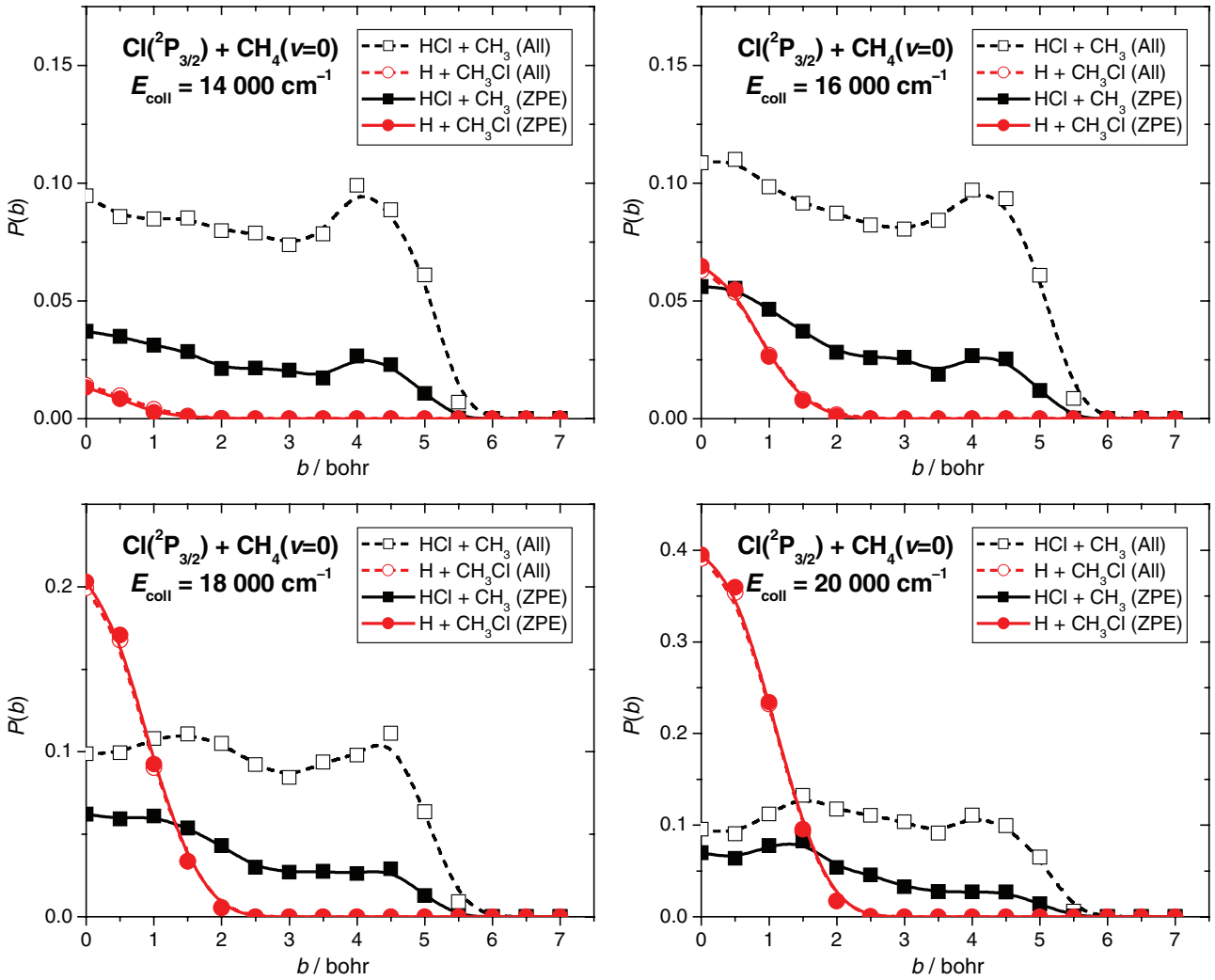

FIG. 6. Probabilities of the Cl(^{2}P$_{3/2}$) + CH_4(v = 0) → HCl + CH_3 and H + CH_3Cl reactions as a function of the impact parameter at different collision energies. The probabilities were obtained considering all the trajectories ("All") as well as ZPE constrained trajectories ("ZPE") in which CH_3 or CH_3Cl has at least zero-point vibrational energy.

probabilities as the above-described constraint based only on the polyatomic products.

B. Reaction probabilities and cross sections (abstraction vs. substitution and SO vs. non-SO)

First, we consider high-energy calculations where the substitution reaction can occur. Reaction probabilities as a function of impact parameter at different E_{coll} in the 14 000–20 000 cm^{-1} range are shown in Fig. 6. Without ZPE constraint the abstraction reaction has about 10% probability at $b = 0$ and this remains nearly constant over a large impact parameter range up to 4.5 bohr, where the probability begins to decay rapidly and vanishes around 6 bohr. The ZPE constraint has a significant effect on the abstraction probabilities, since roughly half of the CH_3 products violate ZPE even at these high collision energies and the ZPE violation is larger as b increases. The substitution channel is just slightly open at E_{coll} = 14 000 cm^{-1} and the probability of substitution increases rapidly as the E_{coll} increases. As Fig. 6 shows, at E_{coll} = 18 000 and 20 000 cm^{-1} the substitution reaction dominates over abstraction at small b, since $P(b = 0)$ is 20% and 40% for the substitution at the above E_{coll}s, respectively. This dominance is even more pronounced if we apply ZPE constraint, since the CH_3Cl products almost never violate ZPE, whereas the abstraction probabilities are much smaller when the constraint is applied. The b dependence of the abstraction and substitution probabilities is very different. For the substitution channel the $P(b)$ decreases rapidly from 0 to b_{max}, where b_{max} is only about 2 bohr. This small b_{max} value is close to the C–H distance in CH_4 or, in other words, b_{max} is roughly the radius of a circle, which goes through 3 H atoms of CH_4. For the abstraction channel, beside the direct rebound mechanism at smaller b, there is also a possibility for abstraction at larger impact parameters via the so-called stripping mechanism. Figure 6 indicates significant reactivity of the abstraction with both mechanisms.

Figure 7 shows the total cross sections for both channels obtained on the non-SO PES as well as on the SO PES. As seen, at low E_{coll} only the HCl + CH_3 channel is open and the H + CH_3Cl channel opens at around 13 000 cm^{-1}.

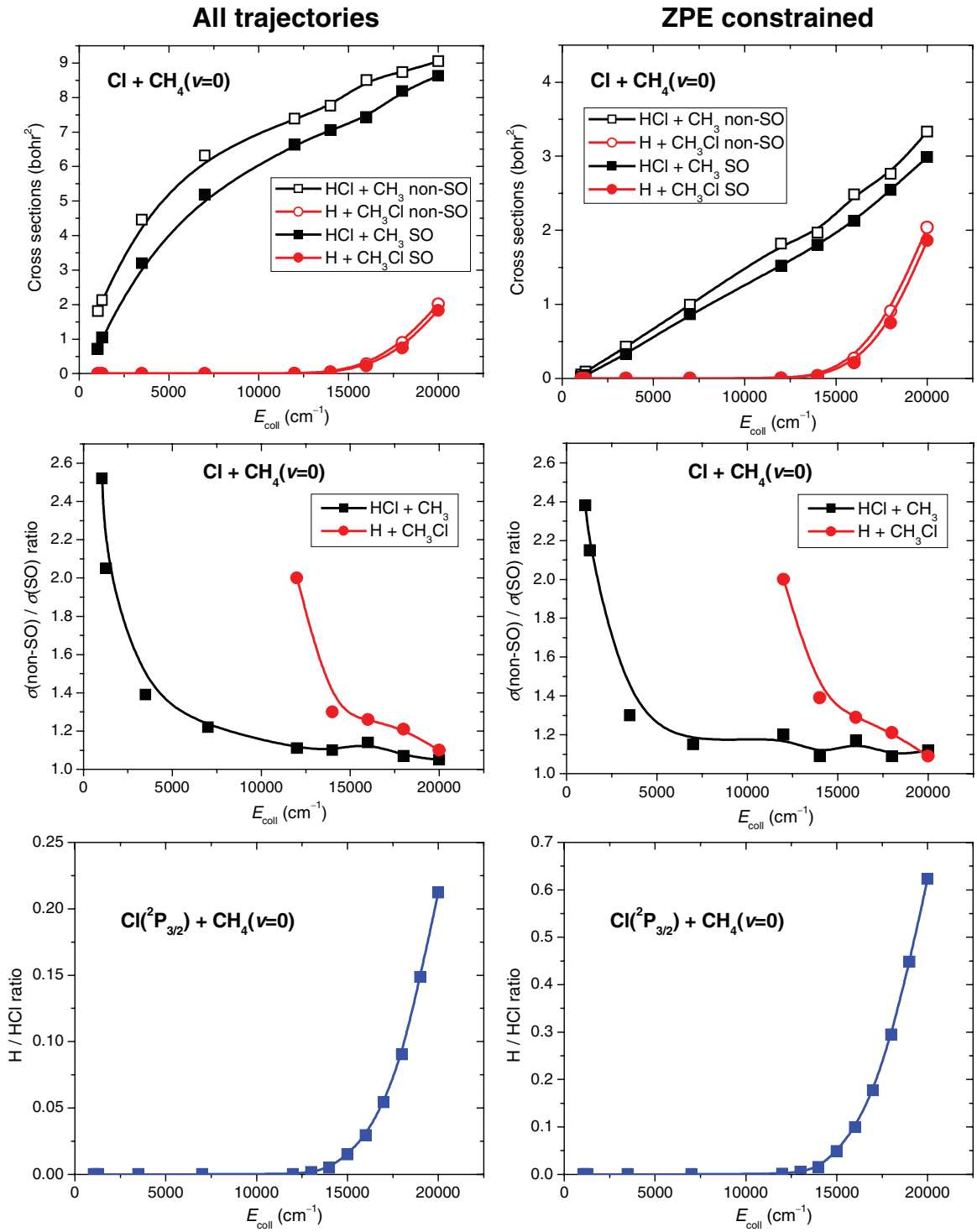

FIG. 7. Cross sections of the Cl + $CH_4(v = 0) \rightarrow$ HCl + CH_3 and H + CH_3Cl reactions on the SO and non-SO PESs (top); ratios of the non-SO and SO cross sections (middle); and ratios of the substitution and abstraction channels on the SO PES (bottom) as a function of collision energy. The cross sections were obtained considering all the trajectories without ZPE constraint (left) as well as ZPE constrained trajectories (right) in which CH_3 or CH_3Cl has at least zero-point vibrational energy.

The H/HCl ratio increases from the threshold and the ratio is around 0.2 at $E_{coll} = 20\,000$ cm^{-1} if all the reactive trajectories are considered. This ratio is very sensitive to the ZPE issue, since only the abstraction channel has significant ZPE violation. Thus, the constrained QCT analysis results in an H/HCl ratio around 0.6 at $E_{coll} = 20\,000$ cm^{-1}. (Note that at $E_{coll} = 20\,000$ cm^{-1} the H/HCl ratio is about 4 at $b = 0$; however, in the integral cross sections the probabilities at larger b dominate favoring the abstraction channel.) The SO correction effectively increases the barrier heights of both channels by 294 cm^{-1}. As a result, we see smaller cross sections on the SO PES relative to those on the non-SO PES. At low E_{coll} the effect is quite significant, since the non-SO/SO cross section ratio is between 2.5 and 1.5 in the E_{coll} range of 1050 and

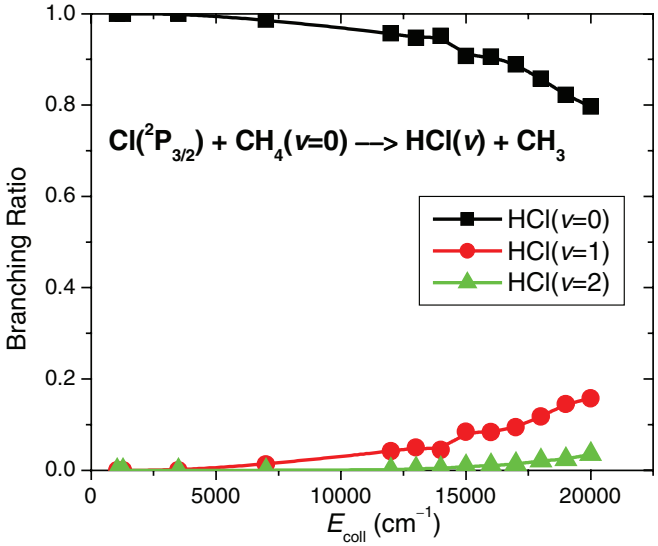

FIG. 8. Normalized HCl vibrational distributions in the $Cl(^2P_{3/2}) + CH_4(v = 0)$ reaction as a function of collision energy. The QCT study employs histogram binning of HCl(v) considering trajectories in which CH_3 has at least zero-point vibrational energy.

3500 cm^{-1}. The ratio tends to 1 as the E_{coll} increases; however, even at E_{coll} = 15 000–20 000 cm^{-1} there is a 10% enhancement on the non-SO PES relative to the cross sections on the SO PES. Even if the substitution reaction has a very high barrier, we see a 10–30% increase of the cross sections when the SO correction is not included in the PES. These non-SO/SO ratios are not sensitive to the ZPE treatment as also shown in Fig. 7 (middle panels).

C. HCl vibrational distributions

The HCl vibrational distributions have been computed as a function of E_{coll}. As Fig. 8 shows, up to about E_{coll} of 7000 cm^{-1} the $Cl(^2P_{3/2}) + CH_4(v = 0)$ reaction produces HCl molecules almost exclusively in the vibrational ground state, although the energetic thresholds for HCl(v = 1) and HCl (v = 2) are 3300 and 6100 cm^{-1}, respectively. These results support a simple vibrationally adiabatic picture, which says that the ground state reactants correlate adiabatically with vibrationally ground state products. (Note that an experiment observed similar results for the $Cl + CHD_3(v = 0) \rightarrow HCl(v) + CD_3(v = 0)$ reaction.[7]) Even at as high E_{coll} as 20 000 cm^{-1}, the population of HCl(v = 0) is still 80% and the minor HCl(v = 1) and HCl(v = 2) states are 17% and 3%, respectively. This is an unusually cold vibrational distribution, especially given that at E_{coll} = 20 000 cm^{-1} vibrational states of HCl are energetically available up to v = 7. Note that the exoergic early-barrier $F + CH_4(v = 0)$ reaction produces vibrationally excited HF products, where the HF(v = 2) is the most populated state (close to 70%) at low collision energies,[8] e.g., E_{coll} = 630 cm^{-1}. At E_{coll} = 20 000 cm^{-1} the available energy in $Cl + CH_4$ is roughly twice than that in $F + CH_4$ at E_{coll} = 630 cm^{-1}; however, the vibrational distribution is much colder in $Cl + CH_4$, showing that the dynamics cannot be explained/predicted based simply on energetics.

D. HCl rotational distributions

Next we consider the HCl(v = 0, J) rotational distributions for the $Cl(^2P_{3/2}) + CH_4(v = 0)$ reaction at different collision energies. These were reported by three experimental groups at a low E_{coll} of 1280 cm^{-1}, showing extremely cold rotational populations.[4–6] QCT studies have been struggling to reproduce this rotational distribution using a variety of PESs and semi-empirical Hamiltonians, and instead produce a too-hot distribution. In a recent paper,[28] it was stated that "...QCT calculations are missing an important dynamical feature that quenches the HCl rotational motion." The conclusion was based on the fact that HCl(v = 0, J) distribution, again quoting from Ref. 28 "is virtually identical to those obtained with the SRP-MSINDO PES and with the high quality *ab initio* PES of Ref. 27." In Fig. 9 we present QCT results obtained by using the current PES and, as seen, the agreement between theory and experiment[6] is excellent, confirming the measurement of Murray *et al.*[6] and Varley and Dagdigian[5] showing the peak feature at J = 1. These results demonstrate that QCT is able to provide good agreement with experiment if an accurate PES is used. Figure 9 also shows that in order to achieve this excellent agreement, a zero-point energy constrained binning has to be used. Nevertheless, even if all the trajectories are considered the rotational distribution still peaks at J = 1, although it has small probabilities even at larger J values. Furthermore, we tested that histogram binning and Gaussian binning [based on Ref. 10] of HCl(v, J) resulted in similar distributions. Here we have reported the statistically more robust results obtained by histogram binning. Regardless of the binning technique employed, the rotational

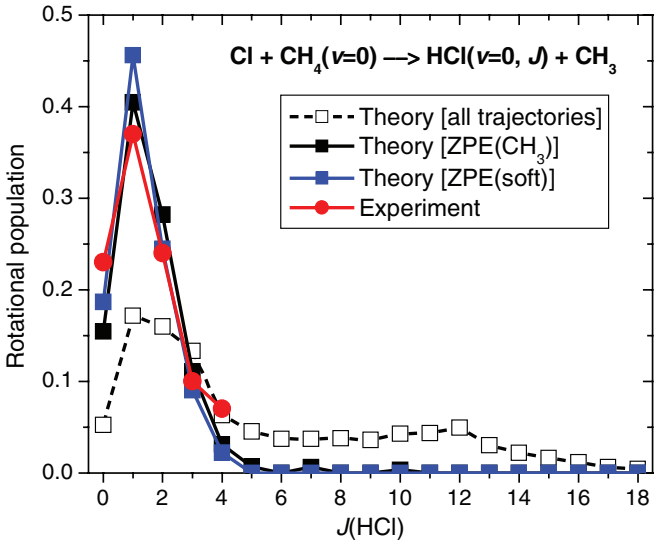

FIG. 9. Normalized HCl(v = 0, J) rotational distributions in the $Cl(^2P_{3/2}) + CH_4(v = 0)$ reaction at E_{coll} = 1280 cm^{-1}. The QCT study considers all the trajectories, ZPE constrained trajectories in which CH_3 has at least zero-point vibrational energy [ZPE(CH_3)], and ZPE constrained trajectories in which $E_{vib}(HCl) + E_{vib}(CH_3)$ is at least ZPE(HCl) + ZPE(CH_3) [ZPE(soft)]. In all cases J was assigned via Eq. (5). Based on the analysis of two batches of trajectories, the estimated statistical uncertainty is less than 15% for the ZPE constrained trajectories and even better when all the trajectories are considered. The experimental results are taken from Ref. 6.

distribution agrees much better with experiment than any previous computed results.

Since only a few HCl rotational states are open, we have investigated the effect of the use of different techniques for obtaining quantized rotational distributions from the classical ones. First, the classical rotational angular momentum j was determined using the center of mass coordinates and momenta of the HCl product in Cartesian space. Second, the quantum number J was assigned by employing three different techniques via

$$j^2 = J(J+1) \Rightarrow J = \text{nint}\left(\sqrt{j^2 + \frac{1}{4}} - \frac{1}{2}\right), \quad (5)$$

$$j^2 = \left(J + \frac{1}{2}\right)^2 \Rightarrow J = \text{nint}\left(j - \frac{1}{2}\right), \quad (6)$$

$$j^2 = J^2 \Rightarrow J = \text{nint}\,(j)\,, \quad (7)$$

where nint denotes rounding to the nearest integer value. Equation (5) is based on the quantum mechanical expression for the eigenvalues of the $\hat{J}^2$ operator as described, for example, in Ref. 55. Equation (6) uses a semi-classical approximation and Eq. (7) is purely classical. In Fig. 10 the HCl rotational distributions are shown obtained by using the above defined three different techniques. The quantum and semi-classical $J(j)$ functions [Eqs. (5) and (6), respectively] converge to each other with increasing J and for $J \geq 2$ virtually no difference is seen between the rotational populations as shown in Fig. 10. For $J = 0$ Eq. (5) gives slightly smaller probability than Eq. (6) does, since Eqs. (5) and (6) assign J to 0 if $j \in (0, 0.87)$ and $(0, 1.00)$, respectively. In contrast, Eq. (7) gives $J = 0$ for $j \in (0, 0.50)$; thus, this third approach provides substantially smaller $J = 0$ population and slightly hotter rotational distributions. As Fig. 10 shows, the HCl

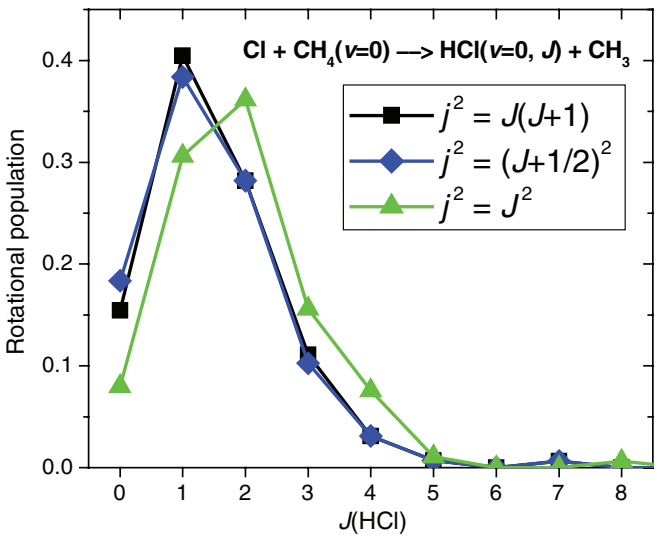

FIG. 10. Normalized HCl($v = 0, J$) rotational distributions in the Cl(^{2}P$_{3/2}$) + CH$_4$($v = 0$) reaction at $E_{\text{coll}} = 1280$ cm^{-1} obtained by three different assignment methods for J as shown in Eqs. (5)–(7). In all cases the QCT study considers ZPE constrained trajectories in which CH$_3$ has at least zero-point vibrational energy.

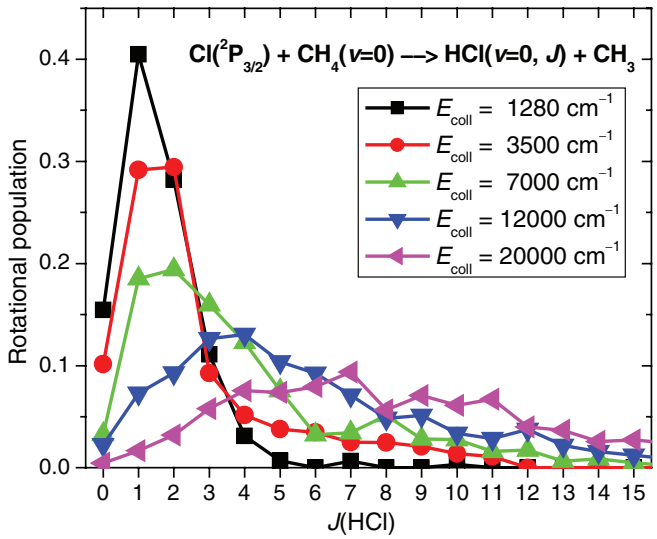

FIG. 11. Normalized HCl($v = 0, J$) rotational distributions in the Cl(^{2}P$_{3/2}$) + CH$_4$($v = 0$) reaction at different collision energies based on trajectories in which CH$_3$ has at least zero-point vibrational energy. In all cases J was assigned via Eq. (5).

rotational distributions obtained by the quantum and semi-classical expressions are virtually identical peaking at $J = 1$, in almost exact agreement with experiment, whereas Eq. (7) shifts the peak to $J = 2$. In our previous studies on F and Cl + CH$_4$,[8,10,18] we employed the quantum expression [Eq. (5)]. Even if we used Eq. (7) for computing the HCl rotational distributions, we would get reasonably good agreement with experiment and much colder distributions than previous QCT studies reported.[28]

In Fig. 11 the HCl($v = 0, J$) rotational distributions are shown at different E_{coll} in the range of 1280–20 000 cm^{-1}. As expected, the distributions become hotter as the E_{coll} increases; however, considering the available energy these distributions are still cold. Even at the high E_{coll} of 7000 and 12 000 cm^{-1} the HCl($v = 0, J$) distributions peak at $J = 2$ and 4, respectively.

The HCl rotational distributions from reactions of Cl with alkanes have been discussed in detail by Murray and Orr-Ewing.[14,56–59] They conclude that a combination of kinematics plus post-transition-state (post-TS) interactions between the incipient HCl plus alkyl products play important roles in the resulting HCl rotational distributions. In the present case, the radical products CH$_3$ and HCl have a strong post TS interaction, as noted above. The favored orientation of this interaction is of C_{3v} symmetry, as shown in Fig. 2, which is exactly the symmetry of the abstraction TS. This symmetry is maintained along the minimum energy path through the exit channel well. Furthermore, the rotation of HCl is significantly hindered in the well even at long CH$_3$–HCl separations, as shown in Fig. 3. The present PES describes this hindering potential very accurately compared to direct *ab initio* CCSD(T)/aug-cc-pVTZ computations as also shown in Fig. 3. Therefore, the exit channel well tends to align the incipient products and thus "counteracts" rotation due to post-TS energy release. An examination of numerous trajectories confirms this and so this post-TS alignment effect is a likely

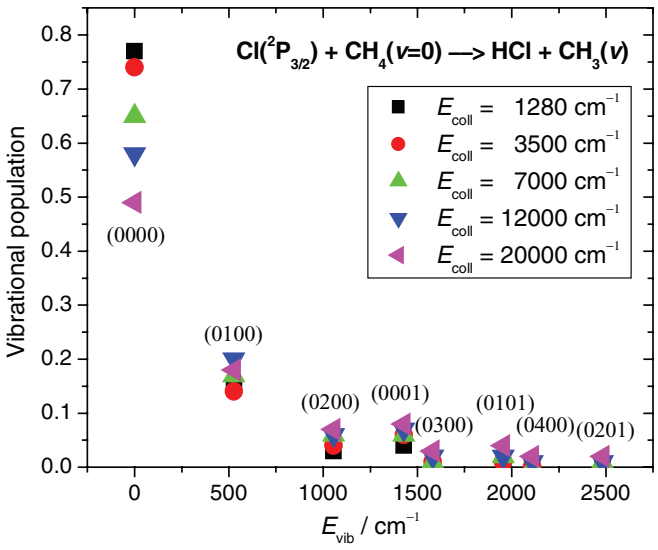

FIG. 12. Normalized mode-specific vibrational distributions for the CH_3 product of the Cl($^2P_{3/2}$) + CH_4($v = 0$) reaction at different collision energies. The assignment of the vibrational states and their Gaussian binning were done based on Ref. 10. The harmonic vibrational energies are relative to the ZPE (6548 cm^{-1}). The harmonic frequencies corresponding to the modes (ω_1, ω_2, ω_3, ω_4) of CH_3 are (3128, 527, 3293, 1428) cm^{-1}. The states shown here correspond to 98%, 99%, 97%, 97%, and 92% of the total CH_3 vibrational populations at collision energies of 1280, 3500, 7000, 12 000, and 20 000 cm^{-1}, respectively.

major contributor to the cold HCl rotational distributions in the Cl + CH_4 reaction.

E. CH_3 mode-specific vibrational distributions

Finally, we have computed mode-specific $CH_3(n_1n_2n_3n_4)$ vibrational distributions for the Cl($^2P_{3/2}$) + CH_4($v = 0$) reaction at different collision energies as shown in Fig. 12. The normal-mode analysis of the CH_3 products and the Gaussian binning, based on the total vibrational energy, of the vibrational states were done as described in detail in Ref. 10. As Fig. 12 shows the CH_3 vibrational distributions are very cold, even at the high E_{coll} of 20 000 cm^{-1} the vibrational ground state is the most populated state and the stretching modes are not excited. The excitation of the bending modes, especially the low frequency umbrella mode (v_2), is seen; however, the populations of the excited states are small. The $CH_3(v_2 = 1)$ state has the most significant population among the excited states; however, $CH_3(v = 0)$ has about 4 times larger population than $CH_3(v_2 = 1)$. At E_{coll} = 1280 cm^{-1} Greaves *et al.*[28] reported similar CH_3 vibrational distributions. They also found no stretching excitations as expected on energy conservation grounds, noted correctly by the authors.[28] Our study reveals that even if we increase E_{coll} to 20 000 cm^{-1}, there is still no stretching excitation, which cannot be simply predicted based on the available energy.

We also checked the rotational distribution of CH_3, which was found to be cold as well. In summary, QCT shows that both the HCl and CH_3 ro-vibrational distributions are very cold even at high collision energies; therefore, most of the available energy is transferred into the translational motion of the products.

V. SUMMARY AND CONCLUSIONS

One of the main challenges of first-principles simulations of the dynamics of polyatomic reactions is the development of the PES, whose accuracy determines the quality of results obtained from nuclear motion calculations using the PES. We have developed an accurate PES for a fundamental polyatomic bimolecular reaction, Cl + methane, based on a permutationally invariant fit to roughly 16 000 *ab initio* electronic energies. The energies were obtained by a composite *ab initio* method based on explicit CCSD(T)/aug-cc-pVDZ, all-electron-MP2/aug-cc-pCVTZ, and MP2/aug-cc-pVDZ computations. We have shown that this composite approach outperforms the computationally more expensive CCSD(T)/aug-cc-pVTZ level of theory; thus, it could be a great help for any future work on similar reactions. Furthermore, we employed spin-orbit and counterpoise corrections for the entrance channel. As a result, the present PES is of unprecedented accuracy, which was proved by comparing stationary-point structures, energetics, and frequencies to new benchmark values.

The global PES describes both the abstraction (HCl + CH_3) and substitution (H + CH_3Cl) channels. Both reactions are endoergic and have late barriers with product-like C_{3v} saddle-point structures. Note that the seemingly similar F + CH_4 abstraction reaction has a very low early barrier with a bent (C_s) saddle point.[8] The new benchmark energetics was obtained by the composite FPA approach.[29,30] We have shown that the CCSD method overestimates the barrier heights by roughly 40% and 10% for the abstraction and substitution reactions, respectively. The "gold standard" CCSD(T) method describes the electron correlation much better, since the above relative discrepancies become only 2% and 1%, respectively, when comparing to CCSDT(Q) results. The basis set effects on the barrier heights are also significant, since the aug-cc-pVTZ basis, which is considered "large" in Cl + CH_4 papers, overestimates the abstraction and substitution barrier heights by roughly 10% and 3%, respectively. The core correlation and scalar relativistic effects turned out to be not significant on the barrier heights and reaction enthalpies, but one must consider the spin-orbit correction, which increases the above-mentioned relative energies by 294 cm^{-1}.

We have performed QCT calculations both on the non-SO and SO ground state PESs. For the first time, we showed that at collision energy of ~13 000 cm^{-1} the substitution channel opens and at collision energy of 20 000 cm^{-1} the H/HCl ratio is about 0.2–0.6 with high sensitivity to the ZPE treatment for the abstraction channel. The two channels have very different impact parameter, b, dependence; the probability of the abstraction reaction at high collision energies is almost b-independent up to b = 4.5 bohr and drops between 4.5 and 6 bohr. On the other hand, the maximal b of the substitution is only 2 bohr and the probability decays rapidly as the b increases from 0 to 2 bohr. The QCT calculations show that the spin-orbit correction decreases the abstraction cross sections by a factor of 1.5–2.5 at low collision energies. Regarding the HCl and CH_3 product state distributions, we have found that the Cl + CH_4($v = 0$) reaction mainly produces HCl($v = 0$) and CH_3($v = 0$) molecules even at high collision energies, where many vibrational states are energetically

available, following a vibrationally adiabatic picture as was previously predicted by an experiment on Cl + $CHD_3(v = 0)$ → HCl(v) + $CD_3(v = 0)$.[7] The HCl($v = 0$, J) rotational distributions have been found to be also cold, in agreement with experiment.[6]

The present study shows that QCT can reproduce experiment if an accurate PES is used. The agreements between the computed and measured HCl rotational distributions and the benchmark and PES energetics suggest that the predictions on the high-collision energy dynamics involving the substitution channel could be a realistic guidance for future experimental investigations. Furthermore, the present high-quality Cl + methane PES opens the door for many future quasiclassical and (at least in reduced dimensionality) quantum nuclear motion computations. These quantum calculations could provide insight into the effects of tunneling and reactive resonances, which could be important at low collision energies. Even if our study demonstrates that the dynamics can be well described on the ground state SO surface, a further direction of future research could consider the development of full-dimensional PESs for the excited SO states allowing study of the non-adiabatic dynamics.

ACKNOWLEDGMENTS

G.C. thanks the National Science Foundation (CHE-0625237) and J.M.B. thanks the Department of Energy (DE-FG02-97ER14782) for financial support.

[1] W. Zhang, H. Kawamata, and K. Liu, Science **325**, 303 (2009).
[2] S. Yoon, R. J. Holiday, and F. F. Crim, J. Phys. Chem. B **109**, 8388 (2005).
[3] R. J. Holiday, C. H. Kwon, C. J. Annesley, and F. F. Crim, J. Chem. Phys. **125**, 133101 (2006).
[4] W. R. Simpson, T. P. Rakitzis, S. A. Kandel, T. Lev-On, and R. N. Zare, J. Phys. Chem. **100**, 7938 (1996).
[5] D. F. Varley and P. J. Dagdigian, J. Phys. Chem. **99**, 9843 (1995).
[6] C. Murray, B. Retail, and A. J. Orr-Ewing, Chem. Phys. **301**, 239 (2004).
[7] S. Yan, Y.-T. Wu, B. Zhang, X.-F. Yue, and K. Liu, Science **316**, 1723 (2007).
[8] G. Czakó, B. C. Shepler, B. J. Braams, and J. M. Bowman, J. Chem. Phys. **130**, 084301 (2009).
[9] G. Czakó and J. M. Bowman, J. Am. Chem. Soc. **131**, 17534 (2009).
[10] G. Czakó and J. M. Bowman, J. Chem. Phys. **131**, 244302 (2009).
[11] G. Czakó, Q. Shuai, K. Liu, and J. M. Bowman, J. Chem. Phys. **133**, 131101 (2010).
[12] D. Troya and P. J. E. Weiss, J. Chem. Phys. **124**, 074313 (2006).
[13] H. A. Bechtel, Z. H. Kim, J. P. Camden, and R. N. Zare, J. Chem. Phys. **120**, 791 (2004).
[14] C. Murray and A. J. Orr-Ewing, Int. Rev. Phys. Chem. **23**, 435 (2004).
[15] J. C. Polanyi, Science **236**, 680 (1987).
[16] G. Czakó and J. M. Bowman, Phys. Chem. Chem. Phys. **13**, 8306 (2011).
[17] W. W. Harper, S. A. Nizkorodov, and D. J. Nesbitt, J. Chem. Phys. **113**, 3670 (2000).
[18] G. Czakó and J. M. Bowman, Science **334**, 343 (2011).
[19] T. N. Truong, D. G. Truhlar, K. K. Baldridge, M. S. Gordon, and R. Steckler, J. Chem. Phys. **90**, 7137 (1989).
[20] J. Espinosa-García and J. C. Corchado, J. Chem. Phys. **105**, 3517 (1996).
[21] T. Joseph, R. Steckler, and D. G. Truhlar, J. Chem. Phys. **87**, 7036 (1987).
[22] J. C. Corchado, D. G. Truhlar, and J. Espinosa-García, J. Chem. Phys. **112**, 9375 (2000).
[23] C. Rangel, M. Navarrete, J. C. Corchado, and J. Espinosa-García, J. Chem. Phys. **124**, 124306 (2006).
[24] H.-G. Yu and G. Nyman, J. Chem. Phys. **111**, 6693 (1999).
[25] S. T. Banks and D. C. Clary, Phys. Chem. Chem. Phys. **9**, 933 (2007).
[26] S. M. Remmert, S. T. Banks, J. N. Harvey, A. J. Orr-Ewing, and D. C. Clary, J. Chem. Phys. **134**, 204311 (2011).
[27] J. F. Castillo, F. J. Aoiz, and L. Bañares, J. Chem. Phys. **125**, 124316 (2006).
[28] S. J. Greaves, R. A. Rose, F. Abou-Chahine, D. R. Glowacki, D. Troya, and A. J. Orr-Ewing, Phys. Chem. Chem. Phys. **13**, 11438 (2011).
[29] W. D. Allen, A. L. L. East, and A. G. Császár, in *Structures and Conformations of Non-Rigid Molecules*, edited by J. Laane, M. Dakkouri, B. van der Veken, and H. Oberhammer (Kluwer, Dordrecht, 1993), p. 343.
[30] A. G. Császár, W. D. Allen, and H. F. Schaefer, J. Chem. Phys. **108**, 9751 (1998).
[31] G. Czakó, E. Mátyus, A. C. Simmonett, A. G. Császár, H. F. Schaefer III, and W. D. Allen, J. Chem. Theory Comput. **4**, 1220 (2008).
[32] G. Czakó, B. Nagy, G. Tasi, Á. Somogyi, J. Šimunek, J. Noga, B. J. Braams, J. M. Bowman, and A. G. Császár, Int. J. Quant. Chem. **109**, 2393 (2009).
[33] O. L. Polyansky, A. G. Császár, S. V. Shirin, N. F. Zobov, P. Barletta, J. Tennyson, D. W. Schwenke, and P. J. Knowles, Science **299**, 539 (2003).
[34] K. A. Peterson and T. H. Dunning, Jr., J. Chem. Phys. **117**, 10548 (2002).
[35] K. Raghavachari, G. W. Trucks, J. A. Pople, and M. Head-Gordon, Chem. Phys. Lett. **157**, 479 (1989).
[36] B. J. Braams and J. M. Bowman, Int. Rev. Phys. Chem. **28**, 577 (2009).
[37] J. M. Bowman, G. Czakó, and B. Fu, Phys. Chem. Chem. Phys. **13**, 8094 (2011).
[38] T. H. Dunning, Jr., J. Chem. Phys. **90**, 1007 (1989).
[39] R. A. Kendall, T. H. Dunning, Jr., and R. J. Harrison, J. Chem. Phys. **96**, 6796 (1992).
[40] D. E. Woon and T. H. Dunning, Jr., J. Chem. Phys. **103**, 4572 (1995).
[41] W. J. Hehre, L. Radom, P. v. R. Schleyer, and J. A. Pople, *Molecular Orbital Theory* (Wiley, New York, 1986).
[42] C. Møller and M. S. Plesset, Phys. Rev. **46**, 618 (1934).
[43] J. Čížek, J. Chem. Phys. **45**, 4256 (1966).
[44] J. D. Watts, J. Gauss, and R. J. Bartlett, J. Chem. Phys. **98**, 8718 (1993).
[45] M. Kállay and J. Gauss, J. Chem. Phys. **123**, 214105 (2005).
[46] H.-J. Werner, P. J. Knowles, R. Lindh, F. R. Manby, M. Schütz *et al.*, MOLPRO, version 2008.1, a package of *ab initio* programs, 2008, see http://www.molpro.net.
[47] MRCC, a string-based quantum chemical program suite written by M. Kállay, for the latest version, see http://mrcc.hu.
[48] M. Kállay and P. R. Surján, J. Chem. Phys. **115**, 2945 (2001).
[49] CFOUR, a quantum chemical program package written by J. F. Stanton, J. Gauss, M. E. Harding, P. G. Szalay with contributions from A. A. Auer, R. J. Bartlett, U. Benedikt, C. Berger, D. E. Bernholdt, Y. J. Bomble, L. Cheng, O. Christiansen, M. Heckert, O. Heun, C. Huber, T.-C. Jagau, D. Jonsson, J. Jusélius, K. Klein, W. J. Lauderdale, D. A. Matthews, T. Metzroth, D. P. O'Neill, D. R. Price, E. Prochnow, K. Ruud, F. Schiffmann, W. Schwalbach, S. Stopkowicz, A. Tajti, J. Vázquez, F. Wang, J. D. Watts; The integral packages MOLECULE, J. Almlöf and P. R. Taylor; PROPS, P. R. Taylor; abacus, T. Helgaker, H. J. Aa. Jensen, P. Jørgensen, and J. Olsen; ECP routines by A. V. Mitin and C. van Wüllen, for the current version, see http://www.cfour.de.
[50] M. Douglas and N. M. Kroll, Ann. Phys. **82**, 89 (1974).
[51] A. Berning, M. Schweizer, H.-J. Werner, P. J. Knowles, and P. Palmieri, Mol. Phys. **98**, 1823 (2000).
[52] A. Karton and J. M. L. Martin, Theor. Chem. Acc. **115**, 330 (2006); W. Klopper and W. Kutzelnigg, J. Mol. Struct.: THEOCHEM **28**, 339 (1986); G. Tasi and A. G. Császár, Chem. Phys. Lett. **438**, 139 (2007).
[53] T. Helgaker, W. Klopper, H. Koch, and J. Noga, J. Chem. Phys. **106**, 9639 (1997).
[54] M. Cheng, Y. Feng, Y. Du, Q. Zhu, W. Zheng, G. Czakó, and J. M. Bowman, J. Chem. Phys. **134**, 191102 (2011).
[55] W. L. Hase, *Encyclopedia of Computational Chemistry* (Wiley, New York, 1998), pp. 399–407.
[56] S. Rudić, C. Murray, J. N. Harvey, and A. J. Orr-Ewing, J. Chem. Phys. **120**, 186 (2004).
[57] C. Murray, J. K. Pearce, S. Rudić, B. Retail, and A. J. Orr-Ewing, J. Phys. Chem. A **109**, 11093 (2005).
[58] J. K. Pearce, C. Murray, P. N. Stevens, and A. J. Orr-Ewing, Mol. Phys. **103**, 1785 (2005).
[59] J. K. Pearce, C. Murray, and A. J. Orr-Ewing, Phys. Scr. **73**, C14 (2006).